The splicing regulator Rbfox2 is required for both cerebellar development and mature motor function

Lauren T. Gehman,[1] Pratap Meera,[2] Peter Stoilov,[3] Lily Shiue,[4] Janelle E. O'Brien,[5] Miriam H. Meisler,[5] Manuel Ares Jr.,[4] Thomas S. Otis,[2] and Douglas L. Black[1,6,7]

[1]Molecular Biology Institute University of California at Los Angeles, Los Angeles, California 90095, USA; [2]Department of Neurobiology, David Geffen School of Medicine, University of California at Los Angeles, Los Angeles, California 90095, USA; [3]Department of Biochemistry, School of Medicine, West Virginia University, Morgantown, West Virginia 26506, USA; [4]Department of Molecular, Cell, and Developmental Biology, Sinsheimer Labs, University of California at Santa Cruz, Santa Cruz, California 95064, USA; [5]Department of Human Genetics, University of Michigan, Ann Arbor, Michigan 48109, USA; [6]Howard Hughes Medical Institute, University of California at Los Angeles, Los Angeles, California 90095, USA

The Rbfox proteins (Rbfox1, Rbfox2, and Rbfox3) regulate the alternative splicing of many important neuronal transcripts and have been implicated in a variety of neurological disorders. However, their roles in brain development and function are not well understood, in part due to redundancy in their activities. Here we show that, unlike Rbfox1 deletion, the CNS-specific deletion of Rbfox2 disrupts cerebellar development. Genome-wide analysis of *Rbfox2*$^{-/-}$ brain RNA identifies numerous splicing changes altering proteins important both for brain development and mature neuronal function. To separate developmental defects from alterations in the physiology of mature cells, Rbfox1 and Rbfox2 were deleted from mature Purkinje cells, resulting in highly irregular firing. Notably, the Scn8a mRNA encoding the $Na_v1.6$ sodium channel, a key mediator of Purkinje cell pacemaking, is improperly spliced in RbFox2 and Rbfox1 mutant brains, leading to highly reduced protein expression. Thus, Rbfox2 protein controls a post-transcriptional program required for proper brain development. Rbfox2 is subsequently required with Rbfox1 to maintain mature neuronal physiology, specifically Purkinje cell pacemaking, through their shared control of sodium channel transcript splicing.

[*Keywords*: Rbfox2/Rbm9; alternative splicing; Purkinje cell; Nav1.6/Scn8a; sodium channels; pacemaking]

Supplemental material is available for this article.

Received November 1, 2011; revised version accepted January 31, 2012.

Alternative pre-mRNA splicing is an important mechanism for regulating gene expression that contributes greatly to proteomic diversity in eukaryotes (Black 2003; Blencowe 2006; Nilsen and Graveley 2010). Changes in exon inclusion or splice site usage can substantially alter the expression or function of the encoded protein. Alternative splicing is especially prevalent in the mammalian nervous system, where it controls aspects of neural tube patterning, synaptogenesis, and the regulation of membrane physiology, among other important processes (Lipscombe 2005; Licatalosi and Darnell 2006; Li et al. 2007). The choice of splicing pattern is generally controlled by *trans*-acting RNA-binding proteins that bind to *cis*-acting elements in the pre-mRNA to enhance or silence particular splicing events (Black 2003; Matlin et al. 2005; Chen and Manley 2009; Nilsen and Graveley 2010). These RNA-binding proteins can be expressed in a temporal- or tissue-specific manner to alter the splicing of a defined set of transcripts. Some of these splicing regulators have been shown to play important roles in the developing and adult mammalian brain (Jensen et al. 2000; Lukong and Richard 2008; Calarco et al. 2009; Yano et al. 2010; Gehman et al. 2011; Raj et al. 2011; Zheng et al. 2012).

In mammals, the RNA-binding Fox (Rbfox) family of splicing regulators is comprised of three members: Rbfox1 (Fox-1 or A2BP1), Rbfox2 (Fox-2 or RBM9), and Rbfox3 (Fox-3, HRNBP3, or NeuN) (Kuroyanagi 2009). Each Fox protein has a single central RNA recognition motif (RRM) RNA-binding domain that recognizes the sequence (U)GCAUG found within introns flanking alternative exons (Jin et al. 2003; Auweter et al. 2006; Ponthier et al. 2006). The position of the (U)GCAUG motif with respect to the alternative exon dictates the effect of the Rbfox proteins on splicing. A motif located downstream from the alternative exon generally promotes Rbfox-dependent exon inclusion, whereas an upstream motif will usually

[7]**Corresponding author.**
E-mail dougb@microbio.ucla.edu.
Article published online ahead of print. Article and publication date are online at http://www.genesdev.org/cgi/doi/10.1101/gad.182477.111. Freely available online through the *Genes & Development* Open Access option.

repress inclusion (Huh and Hynes 1994; Modafferi and Black 1997; Jin et al. 2003; Nakahata and Kawamoto 2005; Underwood et al. 2005; Zhang et al. 2008; Kuroyanagi 2009; Yeo et al. 2009). The three mouse Rbfox paralogs show a high degree of sequence conservation, especially within the RNA-binding domain, which is identical between Rbfox1 and Rbfox2 and only slightly altered in Rbfox3 (94% amino acid identity). The N-terminal and C-terminal domains are less similar between the proteins, presumably allowing for different protein–protein interactions. All three Rbfox family members are highly expressed in most neurons of the mature brain, where they regulate the splicing of neuronal transcripts (McKee et al. 2005; Nakahata and Kawamoto 2005; Underwood et al. 2005; Kim et al. 2009; Tang et al. 2009; Hammock and Levitt 2011). Rbfox1 and Rbfox2 have been shown to control a shared set of neuronal-specific target exons, including exon N30 of nonmuscle myosin heavy chain II-B (NMHC-B), exon N1 of c-*src*, and exons 9* and 33 of the L-type calcium channel $Ca_v1.2$ (Nakahata and Kawamoto 2005; Underwood et al. 2005; Tang et al. 2009).

The individual Rbfox family members show differing patterns of expression. Rbfox1 is expressed in neurons, heart, and muscle, while Rbfox3 is limited to neurons (Wolf et al. 1996; Jin et al. 2003; McKee et al. 2005; Underwood et al. 2005; Kim et al. 2009; Damianov and Black 2010). Rbfox2 is expressed in these tissues as well as other cell types, including the embryo, hematopoietic cells, and embryonic stem cells (ESCs) (Underwood et al. 2005; Ponthier et al. 2006; Yeo et al. 2007). Thus, although the Rbfox proteins can regulate many of the same target exons when ectopically expressed, their in vivo targets may differ due to the variable expression of each protein. For example, Rbfox2 controls the developmental-specific splicing of exons in fibroblast growth factor receptor 2 (FGFR2), erythrocyte protein 4.1R, and STE20-like kinase in cells where the other proteins are absent (Baraniak et al. 2006; Ponthier et al. 2006; Yang et al. 2008; Yeo et al. 2009). Rbfox2 is clearly important for splicing regulation during embryonic growth and development, but its role in the brain is less clear.

Defects in alternative splicing can lead to neurological and neuromuscular disease, such as frontotemporal dementia and myotonic dystrophy (Faustino and Cooper 2003; Licatalosi and Darnell 2006; Cooper et al. 2009). The Rbfox proteins have also been linked to neurological conditions. Human mutations in the *RBFOX1* (*A2BP1*) gene can lead to severe disorders, including mental retardation, epilepsy, and autism spectrum disorder (Bhalla et al. 2004; Barnby et al. 2005; Martin et al. 2007; Sebat et al. 2007; Voineagu et al. 2011). Moreover, human RBFOX1 was first identified through an interaction with Ataxin-2, the protein mutated in spinocerebellar ataxia type II (SCAII), and RBFOX2 was later shown to interact with Ataxin-1, which is mutated in SCAI patients (Shibata et al. 2000; Lim et al. 2006). These results imply a role for Rbfox proteins in cerebellar function.

We recently showed that deletion of *Rbfox1* results in increased neuronal excitation in the hippocampus and seizures in the mouse, in keeping with its regulation of many gene products important for synaptic transmission (Gehman et al. 2011). Rbfox1 mutation did not lead to obvious cerebellar defects. Interestingly, deletion of Rbfox2 did not produce the same seizure phenotype as Rbfox1 deletion. Thus, while the Rbfox proteins share some target exons in the brain, they are not fully redundant in their functions.

To better understand the roles of Rbfox-mediated splicing regulation in the brain, we created mice with tissue- and cell type-specific deletions of one or more Rbfox proteins. We found that CNS-specific deletion of Rbfox2 results in impaired cerebellar development and additional neurological phenotypes, whereas postnatal deletion from cerebellar Purkinje neurons leads to marked deficits in neuronal excitability and, specifically, pacemaking. Thus, like Rbfox1, Rbfox2 is essential for the proper function of mature neural circuits, but also plays a role in brain development.

Results

The Rbfox proteins show differing patterns of expression in the cerebellum

While expression of the Rbfox proteins overlaps in most areas of the brain (Gehman et al. 2011; Kim et al. 2011), the three Rbfox paralogs show strikingly different patterns of expression in neurons of the cerebellum. The cerebellar cortex consists of the internal granule cell layer (iGCL), a middle Purkinje cell layer, and an outermost molecular layer (ML) (Fig. 1A). In the adult wild-type cerebellum, we found that granule cells express Rbfox1 and Rbfox3, but not Rbfox2. Inhibitory neurons of the ML express only Rbfox2. Purkinje cells express Rbfox1 and Rbfox2, but not Rbfox3 (Fig. 1A; Wolf et al. 1996; Kim et al. 2011). In addition to their spatially distinct expression in the adult cerebellum, the Fox proteins exhibit temporally distinct patterns of expression during cerebellar development. Rbfox2 is the earliest Rbfox protein to be expressed, with abundant staining in Purkinje cells, immature cells of the deep cerebellar nuclei, and granule neurons in the iGCL at embryonic day 18 (E18) (Fig. 1B). Rbfox2 expression remains high in Purkinje cells throughout development and adulthood, but cells of the iGCL gradually lose Rbfox2. Most interneurons of the developing and mature ML express Rbfox2. Rbfox1 is first expressed later than Rbfox2, with weak expression in the iGCL by postnatal day 8 (P8), and stronger expression in this region and in Purkinje cells by P14 (Fig. 1B). Rbfox3 is highly expressed in the iGCL by P5 but is never expressed in Purkinje cells (Figs. 1A, 2D). Early in their development, Purkinje cells express only Rbfox2, indicating that this particular Rbfox protein could play a role in their migration and maturation. The Rbfox proteins exhibit different subcellular localization in addition to different anatomical and temporal expression. Rbfox1 shows significant staining in both the cytoplasm and nucleus of Purkinje cells, while Rbfox2 is confined to the nucleus (Fig. 1A,B). These nonredundant patterns of expression and localization in the mature and developing cerebellum suggest that the loss of any one of the Rbfox proteins may manifest most strongly in this region of the brain.

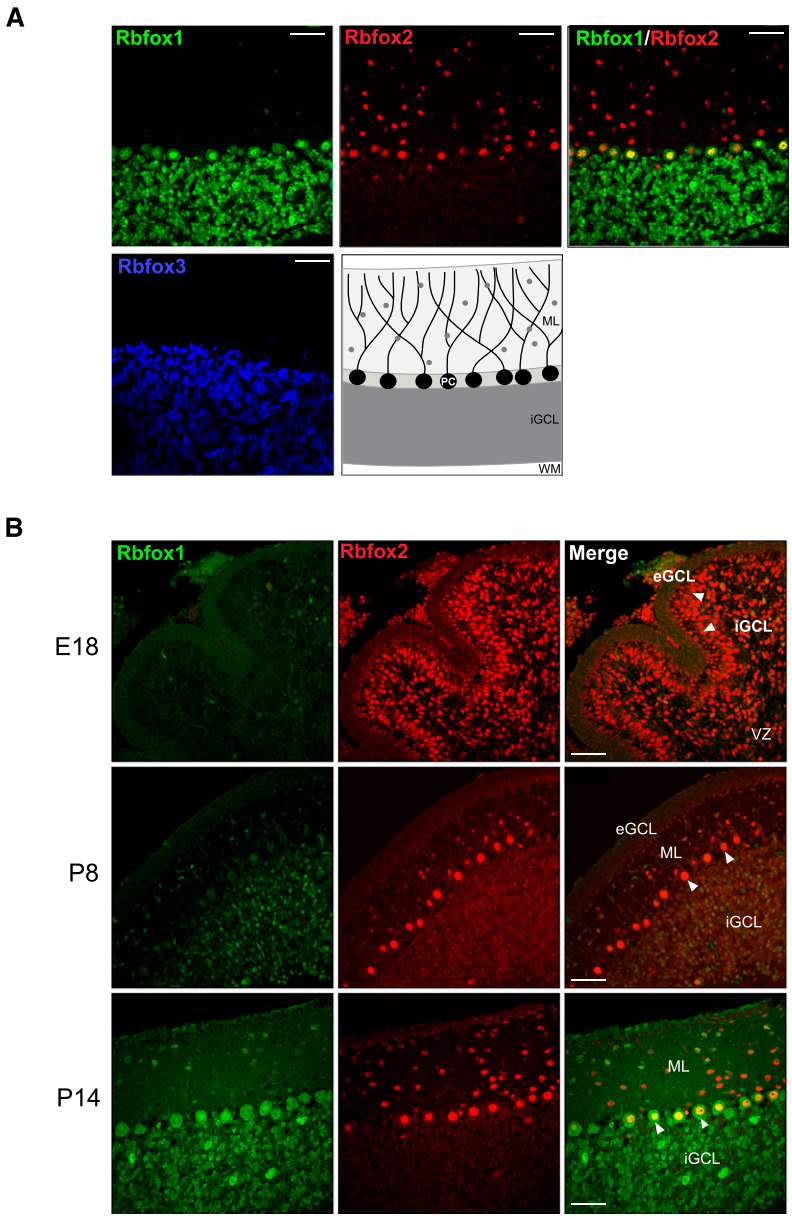

Figure 1. The Rbfox proteins show differing patterns of expression in the wild-type cerebellum. (*A*) Confocal immunofluorescence microscopy on sagittal sections of wild-type (WT) adult cerebellar cortex probed for Rbfox1 (green), Rbfox2 (red), and Rbfox3 (blue) expression; overlayed Rbfox1 and Rbfox2 images are shown in the fourth panel. The fifth panel shows a schematic of the cerebellar cortex; gray circles represent inhibitory interneurons (basket and stellate cells). (*B*) Confocal immunofluorescence microscopy on sagittal sections of wild-type cerebelli at E18, P8, and P14 probed for Rbfox1 and Rbfox2 expression; overlayed images are shown in the far-*right* panels, and arrowheads point to Purkinje cells. (ML) Molecular layer; (PC) Purkinje cell; (iGCL) inner granule cell layer; (WM) white matter; (eGCL) external granule cell layer; (VZ) ventricular zone. Bars, 50 μm.

CNS-specific Rbfox2 results in abnormal cerebellar development

To assess the role of Rbfox2 in brain development and function, we generated mice with CNS-specific deletion of Rbfox2. Mice carrying conditional *Rbfox2* alleles (*Rbfox2*$^{loxP/loxP}$) (Supplemental Fig. 1) were created using standard methods and crossed with mice carrying the Cre recombinase gene driven by the rat *Nestin* promoter and enhancer (*Nestin-Cre*$^{+/-}$). This mouse expresses Cre recombinase in all neural progenitors beginning by E11 (Tronche et al. 1999). The resulting heterozygous *Rbfox2*-$^{loxP/+}$/*Nestin-Cre*$^{+/-}$ mice were again crossed to *Rbfox2*-$^{loxP/loxP}$ mice to obtain homozygous *Rbfox2*$^{loxP/loxP}$/*Nestin-Cre*$^{+/-}$ mice. Cre-mediated recombination deletes *Rbfox2* exons 6 and 7 between the *loxP* sites, resulting in a coding sequence frameshift and subsequent degradation of the Rbfox2 mRNA. This recombination was confirmed in the DNA of the mutant mice (Supplemental Fig. 1). As expected, *Rbfox2*$^{loxP/loxP}$/*Nestin-Cre*$^{+/-}$ animals displayed loss of Rbfox2 protein in the brain (Fig. 2A; Supplemental Fig. 2). Each of the *Rbfox* genes produces multiple protein isoforms arising from different promoters and alternatively spliced exons. In immunoblots of wild-type brain nuclear lysates, the α-Rbfox2 antibody recognized bands corresponding to the two major Rbfox2 isoforms. These proteins were reduced by 95% in the *Rbfox2*$^{-/-}$ brain, which also showed a complete loss of Rbfox2 immunostaining (Fig. 2A; Supplemental Figure 2). Modest changes in expression of the other Rbfox homologs were observed in the *Rbfox2*$^{-/-}$ brain, with a slight increase (+12%) in the multiple Rbfox1 protein isoforms and a slight decrease

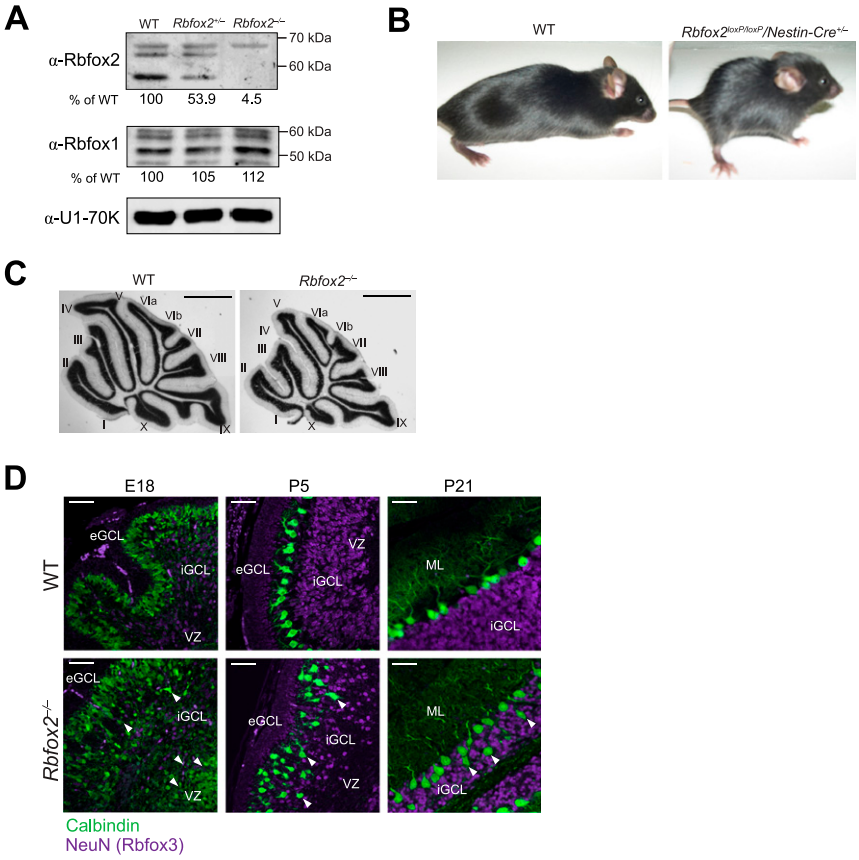

Figure 2. *Rbfox2*$^{loxP/loxP}$/*Nestin-Cre*$^{+/-}$ mice are prone to hydrocephalus and possess abnormal cerebellar morphology. (*A*) Immunoblot analysis of Rbfox2 and Rbfox1 in nuclear lysates isolated from wild-type (WT), *Rbfox2*$^{+/-}$, and *Rbfox2*$^{-/-}$ brains. U1-70K was used as a loading control for total nuclear protein. *Below* each gel is the amount of Rbfox2 or Rbfox1 protein in each sample as a percentage of wild type, normalized by U1-70K expression. Note that the *Rbfox1* and *Rbfox2* genes produce multiple protein isoforms that react with the antibodies. The *top* band in the Rbfox2 panel is nonspecific and was not used in quantification of Rbfox2 levels. (*B*) Wild-type and *Rbfox2*$^{loxP/loxP}$/*Nestin-Cre*$^{+/-}$ mice at 2 mo of age. (*C*) Representative Nissl stains of wild-type and *Rbfox2*$^{-/-}$ cerebelli at 1 mo. Bar, 1 mm. (*D*) Confocal immunofluorescence microscopy on sagittal sections of wild-type and *Rbfox2*$^{-/-}$ cerebelli probed for Calbindin (green) and Rbfox3 (also known as NeuN; purple) expression at E18, P5, and P21. Bar, 50 μm. Arrowheads point to ectopic Purkinje cells. (eGCL) External granule cell layer; (iGCL) internal granule cell layer; (VZ) ventricular zone; (ML) molecular layer.

(−12%) in Rbfox3 (Fig. 2A; data not shown). This is in contrast to Rbfox1 mutant mice that exhibit strong up-regulation of Rbfox2 (Gehman et al. 2011).

The *Rbfox2*$^{loxP/loxP}$/*Nestin-Cre*$^{+/-}$ mice are viable, but homozygous males fail to thrive, and >40% (nine out of 22) die by 1 mo of age. At weaning age (P21), male homozygotes have only 44% the body weight of wild-type males, are very weak, and exhibit a hunched posture. Homozygous females fare slightly better than their male counterparts, with zero dying within the first postnatal month. At P21, female homozygotes are 59% the body weight of wild-type females. The source of this gender difference is not clear. Of the *Rbfox2*$^{loxP/loxP}$/*Nestin-Cre*$^{+/-}$ males and females that survive the first 4 wk, 36% (12 out of 33) develop hydrocephalus with an overtly "domed" head at 8–12 wk of age (Fig. 2B). This severe neurological condition, which required euthanasia, was never observed in heterozygous or wild-type littermates.

Histological analysis by Nissl staining at various postnatal stages prior to the onset of hydrocephalus revealed that the *Rbfox2*$^{-/-}$ cerebellum is reduced in size relative to other brain structures (Fig. 2C). By immunofluorescent staining, we found that the *Rbfox2*$^{-/-}$ cerebellar cortex is abnormal, with >10% of Calbindin-expressing Purkinje cells ectopically located within the iGCL at P10 (Fig. 2D; Supplemental Fig. 3A). During normal cerebellar development, Purkinje cells have completed their migration and are aligned just below the external GCL (eGCL) by E18 (Fig. 2D). In contrast, the E18 *Rbfox2*$^{-/-}$ cerebellum has numerous Purkinje cells that remain near their origin at the ventricular zone (Fig. 2D), suggesting a defect in Purkinje cell radial migration. Purkinje cell migration depends on the Reelin signaling pathway (Miyata et al. 1997), which also controls neuronal migration in other brain areas, such as the cerebral cortex. However, the cortical layers appear morphologically normal in the *Rbfox2*$^{-/-}$ brain (data not shown). At P5, there are ~20% more total Purkinje cells per unit area in the *Rbfox2*$^{-/-}$ cerebellum compared with wild type. At later postnatal stages, the total number of Purkinje cells does not differ between the two genotypes (Supplemental Fig. 3B), indicating that the excess Purkinje cells have been eliminated. To quantify cell death in the cerebellum, we performed terminal deoxynucleotidyltransferase-mediated dUTP-biotin nick end-labeling (TUNEL) staining. We found a threefold increase in TUNEL-positive cells per unit area in the *Rbfox2*$^{-/-}$ cerebellum compared with wild type at P5 (Supplemental Fig. 3C). These TUNEL-positive cells do not clearly coexpress the Purkinje cell marker Calbindin and may represent either granule cells or dying Purkinje cells that have lost Calbindin expression. They presumably include some of the excess Purkinje cells seen at this time that failed to migrate properly.

At later stages of development, *Rbfox2*$^{-/-}$ Purkinje cells show additional abnormalities. After migration, Purkinje cells extend dendritic trees into the ML, where they mature and elaborate postnatally. At P10, the width of the ML is significantly decreased in the *Rbfox2*$^{-/-}$

cerebellum, suggesting a reduction in Purkinje cell dendritic arborization ($P = 0.002$) (Lobe VI in Supplemental Fig. 3D). The reduced size of the *Rbfox2*$^{-/-}$ cerebellum also suggests that there is a decrease in granule cell number, as a result of either reduced proliferation or reduced migration/survival. Under wild-type conditions, developing Purkinje cells secrete growth factors, such as Sonic hedgehog (Shh), to promote the proliferation and survival of granule cell precursors in the eGCL, which then become post-mitotic and migrate to the iGCL (Wang and Zoghbi 2001). Bromodeoxyuridine (BrdU) incorporation assays revealed a minor decrease in cell proliferation in the eGCL, with 10% fewer labeled nuclei 2 h after BrdU injection ($P = 0.021$). In contrast, after 72 h, the number of the BrdU-positive cells in the iGCL of the *Rbfox2*$^{-/-}$ cerebellum was greatly reduced (40% decrease, $P = 0.005$), indicating that depletion of Rbfox2 affects the migration and survival of granule cells (Supplemental Fig. 3E).

Rbfox2$^{loxP/loxP}$/*Nestin-Cre*$^{+/-}$ mice show abnormal posture and difficulty with locomotion as their condition worsens with age. Because most animals die or develop hydrocephalus at a relatively young age, it was not possible to perform quantitative behavioral testing on these mice to assess their motor function. However, the abnormal cerebellar morphology of these mice indicates that they likely possess significant motor impairment (see below).

The Rbfox2$^{-/-}$ *brain exhibits numerous splicing changes in transcripts important for development and mature neuronal function*

We next assayed the changes in splicing in the *Rbfox2*$^{-/-}$ brain compared with wild type. By RT–PCR, we directly assayed candidate exons that are known to be regulated by Rbfox or to possess nearby Rbfox-binding sites. We also used Affymetrix exon junction (MJAY) microarrays to assay transcript abundance and alternative splicing across the genome. Splicing changes in cassette or mutually exclusive exons identified by the array were reassessed by RT–PCR. In total, we identified 29 cassette exons or mutually exclusive exon pairs that changed in inclusion by >5% in the 1-mo-old *Rbfox2*$^{-/-}$ brain compared with wild type (Fig. 3; Table 1; Supplemental Fig. 4).

To assess whether these exons could be directly regulated by an Rbfox protein, we identified (U)GCAUG motifs within the intron sequences 300 nucleotides (nt) downstream or 300 nt upstream (Table 1). These motifs are enriched in the knockout-responsive exons, with many conserved across mammalian species (Table 1; Materials and Methods). The presence of conserved downstream motifs correlated with decreased splicing in the knockout mice. Exons showing increased splicing also generally had upstream motifs that could act as splicing repressor elements (Table 1). However, the direction of the splicing change was not in all cases predictable from the position of binding motifs. As described previously, exons can carry Rbfox-binding motifs both upstream and downstream and/or within the exon (Tang et al. 2009). In some transcripts, exons without nearby Rbfox sites can have more distal sites that are active (Huh and Hynes 1994; Lim and Sharp 1998; Tang et al. 2009). There is also evidence that Rbfox proteins can be recruited to non-UGCAUG elements via interactions with other proteins (Yeo et al. 2009; A Damianov and DL Black, unpubl.). Thus, direct regulation by Rbfox proteins is also not always predictable by sequence alone. The conservation of the proximal binding elements and the correlation of their location with the direction of the splicing changes indicate that most of the observed splicing events are directly regulated by Rbfox2. However, these changes

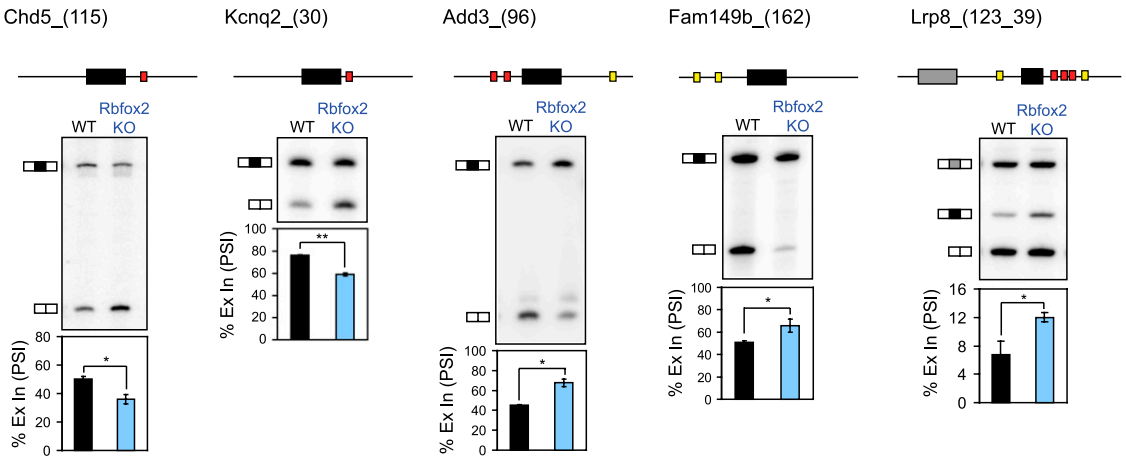

Figure 3. The *Rbfox2*$^{-/-}$ brain exhibits splicing changes of exons with adjacent Rbfox-binding sites. Representative denaturing gel electrophoresis of RT–PCR products for Rbfox2-dependent exons. *Above* each gel is a schematic indicating the alternative exon (horizontal black boxes) and the location of (U)GCAUG binding sites (red and yellow boxes) in the flanking introns (thin horizontal lines). Red boxes indicate (U)GCAUG sites conserved across multiple vertebrate species (Phastcons score >0.5). Shown *below* the gel is a graph quantifying the mean percentage of alternative exon inclusion (percent spliced in, PSI) in wild-type (WT; black bars) and *Rbfox2*$^{-/-}$ (blue bars) brains. Error bars represent SEM; $n = 3$. (*) $P < 0.05$; (**) $P < 0.005$; (*n.s.*) not significant by paired, one-tailed Student's *t*-test. Exact *P*-values are shown in Table 1.

Table 1. *Summary of differentially spliced exons in the Rbfox2$^{-/-}$ brain*

	Alternative event ID	MJAY ratio[a]	RT–PCR ΔPSI[b] (Mean ± SEM)	*P*-value[c]	Upstream (U)GCAUG[d]	Downstream (U)GCAUG[d]	Function[e]	Fox-1 knockout ΔPSI (Mean ± SEM)[f]
1	Traf6 (203)	−1.03	−37 ± 7.0	1.7×10^{-2}	np	np	E3 ubiquitin ligase	–
2	Stx3 (46)	−1.06	−28 ± 1.2	9.5×10^{-4}	−101, −74	+25, +185, +195	SNARE complex	−33 ± 3.7
3	Cacna1s (57)	—	−17 ± 5.2	4.0×10^{-2}	np	**+13**, +44, +60, **+69**, +165	Ion channel	−22 ± 2.6
4	Kcnq2 (30)	—	−17 ± 1.3	2.8×10^{-3}	np	**+9**	Ion channel	–
5	Poldip3 (87)	−1.17	−17 ± 3.7	2.2×10^{-2}	−110	+40	RNA binding	–
6	Camta1 (31)	−0.81	−16 ± 3.7	2.5×10^{-2}	np	**+70, +210, +252**	Calmodulin binding	−22 ± 1.9
7	Chd5 (115)	−0.96	−14 ± 1.9	9.1×10^{-3}	np	**+26**	Chromatin modification	–
8	Snap25 (118)	—	−12 ± 2.7	2.1×10^{-2}	np	**+94**, **+101**, +287	SNARE complex	−24 ± 3.3
9	Gabrg2 (24)	—	−12 ± 3.3	3.3×10^{-2}	np	**+30**	Neurotransmitter receptor	−14 ± 2.1
10	Cacna1d (104)	−0.86	−11 ± 2.2	1.8×10^{-2}	−225, −191	**+93**	Ion channel	+7.6 ± 2.4
11	Larp5 (252)	−1.10	−11 ± 3.4	4.5×10^{-2}	−64	np	Translation	–
12	Cadps (147)	—	−10 ± 2.2	2.2×10^{-2}	−227	**+49**	SNARE complex	−6.1 ± 1.5
13	Epb4.1l3 (117)	−0.83	−10 ± 0.75	2.8×10^{-2}	**-53**	**+40**, +47	Cytoskeletal dynamics	—
14	Csde1, (93)	−0.89	−9.3 ± 2.6	3.5×10^{-2}	**−136**	np	RNA binding	—
15	Huwe1 (234)	−1.25	−7.2 ± 1.7	2.6×10^{-2}	−104	np	E3 ubiquitin ligase	—
16	Scn8a (92)[g]	—	−5.5 ± 1.0	1.7×10^{-2}	np	**+114**, **+192**	Ion channel	−12 ± 0.8
17	Nrxn3 (27)	—	−5.2 ± 1.2	2.4×10^{-2}	np	np	Synapse assembly	−7.6 ± 1.3
18	Cask (36)	+0.92	+5.2 ± 1.7	4.7×10^{-2}	np	np	Synapse assembly	—
19	Lrp8 (39)	—	+5.3 ± 1.2	2.3×10^{-2}	−212	**+21**, **+58**, **+69**, +94, +148	Reelin binding	—
20	Nrcam (57)	—	+6.0 ± 1.8	3.8×10^{-2}	−136	+171	Synapse assembly	+5.5 ± 0.7
21	Epb4.9 (75)	+0.98	+6.8 ± 1.9	3.5×10^{-2}	−35	+100	Cytoskeletal dynamics	—
22	Fubp1 (63)	+1.01	+8.3 ± 2.2	3.3×10^{-2}	np	np	Transcription	—
23	Pbrm1 (156)	—	+9.2 ± 1.9	2.0×10^{-2}	**−78**, **−44**, **−31**	+233	Chromatin modification	+13 ± 2.5
24	Cacna1b (63)	—	+9.3 ± 0.93	4.9×10^{-3}	**−11**	+141	Ion channel	—
25	Mett10d (66)	+0.94	+9.4 ± 1.3	9.6×10^{-3}	np	+36	Chromatin modification	—
26	Dkk3 (84)	+0.88	+11 ± 1.5	9.1×10^{-3}	np	np	Wnt signaling	—
27	Kcnd3 (57)	+1.55	+14 ± 3.1	3.2×10^{-2}	**−16**	**+83**	Ion channel	+28 ± 7.6
28	Fam149b (162)	+1.19	+15 ± 4.2	3.5×10^{-2}	−253, −165	np	Unknown	—
29	Add3 (96)	+1.10	+23 ± 4.3	1.7×10^{-2}	**−122**, **−33**	+242	Cytoskeletal dynamics	—

RT–PCR for each alternative event was performed on *Rbfox2*$^{-/-}$ whole brains, and the relative mean percent change in exon inclusion from the wild-type brain was calculated. The number in parentheses after the gene ID indicates the size in nucleotides of the alternative exon. The events listed are alternative cassette exons, except for Snap25, Cacna1d, Scn8a, and Lrp8, which are mutually exclusive exons. For these events, the downstream exon is listed.

[a]MJAY ratio is a measure of the difference in the average ratio of inclusion to skipping for the indicated exon in the knockout sample group compared with wild type, calculated as previously described (Sugnet et al. 2006). Dashes indicate candidate exons that were directly tested by RT–PCR and were not identified by the array.

[b](ΔPSI) Percent change in exon inclusion (percent spliced in). For mutually exclusive exons, the number given is for the downstream exon.

[c]RT–PCR *P*-value was determined by paired, one-tailed Student's *t*-test ($n = 3$).

[d]Locations of (U)GCAUG-binding sites in the proximal 300 nt upstream of and downstream from the alternative exon are shown with distance in nucleotides. (np) Not present. Bold numbers indicate evolutionarily conserved sites (vertebrate conservation >0.5 as determined by phastCons, http://genome.ucsc.edu).

[e]Reported function of the encoded protein.

[f]ΔPSI values from RT–PCR performed on *Rbfox1*$^{-/-}$ whole brains, as reported previously (Gehman et al. 2011). Dashes indicate no significant change compared with wild type.

[g]The Scn8a (92) entry corresponds to mutually exclusive exons 5N/5A; Scn8a exons 18N/18A were not significantly altered in the *Rbfox2*$^{-/-}$ whole-brain sample, but were changed in the *Rbfox1*$^{+/-}$, *Rbfox2*$^{-/-}$ double mutant cerebellum (see Fig. 6).

were measured in young adult mice that have developed in the absence of Rbfox2, and it is likely that some splicing changes are indirect effects of Rbfox2 depletion. Notably, beside the expected decrease in Rbfox2 transcripts, there were no significant changes in transcript abundance detected in the *Rbfox2*$^{-/-}$ brain. Thus, the effect of Rbfox2, whether direct or indirect, is largely post-transcriptional. Note that initial results from cross-linking immunoprecipitation (CLIP) experiments examining Rbfox1 and Rbfox3 binding in vivo indicate that many of the expected elements are binding at least one Rbfox protein. However, a more extensive Rbfox2 CLIP analysis in mouse cerebelli will be needed to define the direct Rbfox2 targets within the larger cerebellar program of Rbfox-dependent splicing.

Some transcripts altered in the *Rbfox2*$^{-/-}$ knockout were previously shown by CLIP to be bound by Rbfox2 in human ESCs (Yeo et al. 2009), indicating that mouse brains and human ESCs share some Rbfox2-regulated transcripts. However, most transcripts identified in the human ESC Rbfox2 CLIP study are not expressed in adult brains. We also tested by RT–PCR several additional orthologous transcripts expressed in both human ESCs and mouse brains that were identified as Rbfox2 targets in ESCs but not in our microarray analysis (*Picalm*, *Ptbp2*, *Rims2*, *Slk*, and *Tsc2*) (Yeo et al. 2009). None of these exons were differentially spliced between wild-type and *Rbfox2*$^{-/-}$ brains (data not shown), indicating that Rbfox2 regulates these transcripts specifically in human ESCs, perhaps due to the absence of other Rbfox proteins in these cells.

Comparing the results from the two knockout mice helps identify common and specific targets for the two Rbfox proteins. Many exons altered in the Rbfox2 knockout were unchanged in the Rbfox1 knockout brain, indicating that they are either specifically regulated by Rbfox2 or expressed in cells that contain only Rbfox2. For example, exons in the chromodomain helicase *Chd5* and the voltage-gated potassium channel $K_v7.2$ (*Kcnq2*) have downstream Rbfox-binding sites and display decreased inclusion in the *Rbfox2*$^{-/-}$ brain (Fig. 3). Conversely, alternative exons with an upstream (U)GCAUG motif in the γ-adducin gene (*Add3*) and the *Fam149b* gene display increased inclusion in the *Rbfox2*$^{-/-}$ brain (Fig. 3). Twelve splicing changes previously identified in the *Rbfox1*$^{-/-}$ brain (Gehman et al. 2011) were also found in the *Rbfox2*$^{-/-}$ brain, and 11 of these changes occur in the same direction in the two mutants. The exception is a pair of mutually exclusive exons from the *Cacna1d* gene, encoding the L-type calcium channel $Ca_v1.3$. *Cacna1d* exon 8B splicing shows a modest decrease in the *Rbfox2*$^{-/-}$ brain and a small increase in the *Rbfox1*$^{-/-}$ brain compared with wild type (Table 1; Gehman et al. 2011). In the *Rbfox1*$^{-/-}$ brain, the splicing changes were primarily in transcripts involved in synaptic transmission (Gehman et al. 2011). The *Rbfox2*$^{-/-}$ brain shows similar changes in transcripts for ion channels and components of the synaptic machinery, but also in gene products with more diverse functions, such as RNA-binding proteins, transcription factors, and proteins mediating chromatin modification. These Rbfox2-specific targets include a methyltransferase domain-containing protein (*Mett10d*), Polybromo 1 (*Pbrm1*), and the aforementioned Chd5 (Table 1; Supplemental Fig. 4).

Some transcripts whose splicing is altered in the *Rbfox2*$^{-/-}$ brain have been previously implicated in brain development and might contribute to the observed developmental defects in the *Rbfox2*$^{-/-}$ brain. Chd5 is a tumor suppressor with high expression in human fetal brains and adult cerebelli (Thompson et al. 2003). Add3 is involved in cytoskeletal dynamics. Similar to the *Rbfox2*$^{loxP/loxP}$/*Nestin-Cre*$^{+/-}$ mice, mice lacking Adducin proteins develop lethal hydrocephalus due to disrupted cerebral spinal fluid homeostasis (Robledo et al. 2008). We also identified changes in the transcript for low-density lipoprotein receptor-related protein 8 (Lrp8), which binds the protein Reelin to control cortical and Purkinje neuron migration during development (Rice and Curran 2001). Deletion of Lrp8 is known to cause Purkinje cell ectopias and aberrant cerebellar development (Larouche et al. 2008). We found that a 39-nt exon of the Lrp8 transcript is a modestly increased inclusion in the *Rbfox2*$^{-/-}$ brain (Fig. 3). This exon introduces a furin cleavage site into the protein to generate a secreted isoform that acts as a dominant-negative inhibitor of Reelin signaling (Koch et al. 2002). The amount of this dominant-negative isoform is doubled in the *Rbfox2*$^{-/-}$ brain (Fig. 3), but it is not clear whether this would be sufficient to disrupt Reelin signaling and contribute to the observed Purkinje cell migration defect. Each aspect of the *Rbfox2*$^{-/-}$ phenotype is potentially caused by a combination of splicing changes, and dissection of this pleiotropic phenotype will be challenging. Individual defects will need to be complemented by specific mRNA isoforms that may not allow full reversion (Ruggiu et al. 2009; Yano et al. 2010). In summary, numerous splicing changes were identified in the *Rbfox2*$^{-/-}$ brain that could contribute to its aberrant development.

Severe phenotypes of Rbfox1 and Rbfox2 double mutant mice

Compared with other splicing factor knockouts and the number of expected Rbfox targets from CLIP and bioinformatics studies (Ule et al. 2005; Yeo et al. 2009), the splicing changes in *Rbfox1*$^{-/-}$ or *Rbfox2*$^{-/-}$ brains are limited in number and often magnitude, presumably because of redundancy. Consistent with this, the double deletion of Rbfox1 and Rbfox2 in the CNS exhibits a much more severe phenotype than either single knockout. *Rbfox1*$^{loxP/loxP}$/ *Rbfox2*$^{loxP/loxP}$/*Nestin-Cre*$^{+/-}$ mice die perinatally, and we were unable to obtain analyzable sections from these brains at E18 due to tissue fragility. Thus, proper postnatal brain function and development require at least Rbfox1 or Rbfox2. Some compound *Rbfox*/*Nestin* mutants, such as *Rbfox1*$^{+/loxP}$/*Rbfox2*$^{+/loxP}$/*Nestin-Cre*$^{+/-}$ (heterozygous for both Rbfox1 and Rbfox2) or *Rbfox1*$^{loxP/loxP}$/*Rbfox2*$^{+/loxP}$/*Nestin-Cre*$^{+/-}$ (homozygous null for Rbfox1, heterozygous for Rbfox2) are born and develop grossly normal brain architecture. In contrast, *Rbfox1*$^{+/loxP}$/*Rbfox2*$^{loxP/loxP}$/*Nestin-Cre*$^{+/-}$ mice

(heterozygous for Rbfox1 and null for Rbfox2 in the brain) are viable but very small and develop severe ataxia by the second postnatal week (Supplemental Movie 1). Ninety-three percent (56 of 60) of these mice die or require euthanasia due to immobility by 3–4 wk of age. The *Rbfox1*$^{+/-}$/*Rbfox2*$^{-/-}$ cerebellum closely resembles that of the *Rbfox2*$^{-/-}$ cerebellum, being disproportionately small and possessing many ectopic Purkinje cells (data not shown). The enhanced phenotype of the combined *Rbfox1* heterozygote/*Rbfox2*-null mouse supports the idea that Rbfox2 is needed both during development and in the adult, where it is partially redundant with Rbfox1.

Purkinje cell-specific deletion of Rbfox1 and Rbfox2 results in impaired motor function and abnormal Purkinje cell pacemaking

The Rbfox1 protein is primarily expressed late in development and is required for mature neuronal function. The developmental phenotype of the Rbfox2 deletion complicates assessment of its role in the mature brain and its possible redundancy with Rbfox1 and Rbfox3. To examine Rbfox2 function after cerebellar maturation, we used additional Cre lines. Since Purkinje cells are unusual in not expressing the third Rbfox homolog, Rbfox3 (Fig. 1A; Wolf et al. 1996), the loss of Rbfox1 and Rbfox2 could have more severe consequences in these cells. Thus, we created a Purkinje cell-specific double-knockout (DKO) mouse using the Purkinje cell-specific *L7/Pcp2* promoter to drive Cre recombinase expression (Barski et al. 2000). This allowed assessment of Rbfox protein function specifically in these cells.

Rbfox1$^{loxP/loxP}$/*Rbfox2*$^{loxP/loxP}$/*L7-Cre*$^{+/-}$ (L7-DKO) mice were viable and did not exhibit the abnormal cerebellar development or severe ataxia of *Rbfox1*$^{+/loxP}$/*Rbfox2*$^{loxP/loxP}$/*Nestin-Cre*$^{+/-}$ mice. The *L7* promoter is active relatively late in development, with maximal genomic recombination by 2–3 wk of age (Barski et al. 2000). Assessing Rbfox1 and Rbfox2 expression in the L7-DKO cerebellum by confocal immunofluorescence, we found that Purkinje cells continue to express both Rbfox proteins at P20 (Fig. 4A). However, by P70, L7-DKO Purkinje cells no longer express the Rbfox proteins (Fig. 4A), in keeping with the expected timing of gene loss. Purkinje cell morphology in L7-DKO mice at P20 and P70 closely resembled that of wild-type Purkinje cells (Fig. 4B).

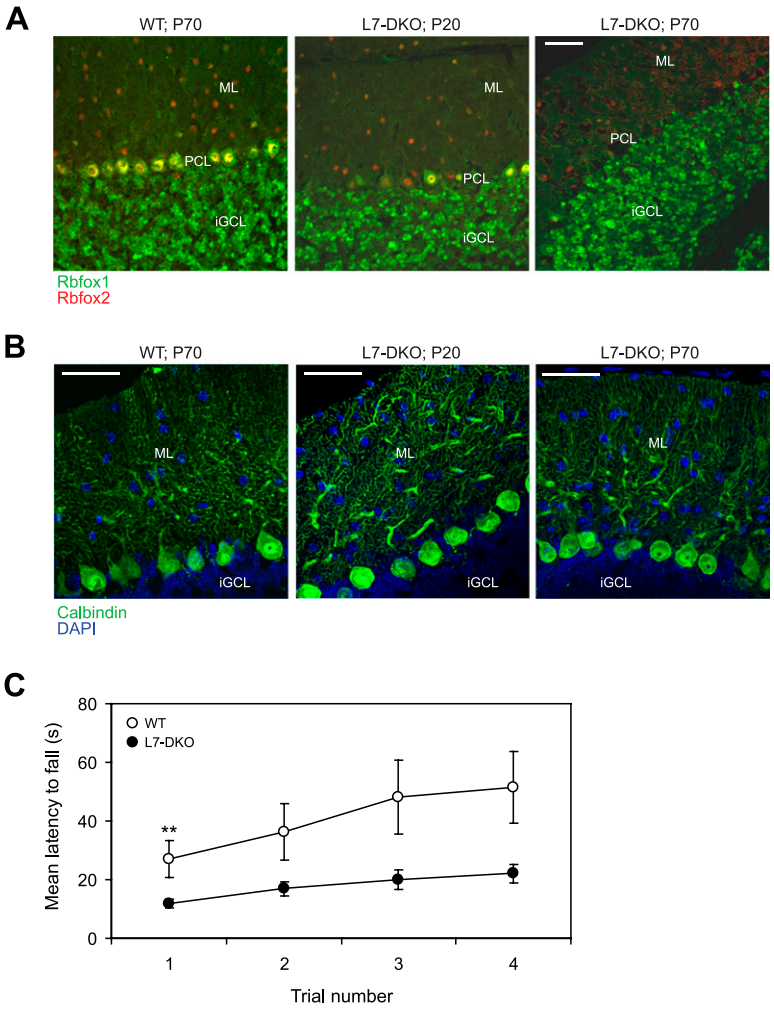

Figure 4. At P70, L7-Cre DKO mice no longer express Rbfox1 and Rbfox2 in Purkinje cells and exhibit impaired motor function. (*A*,*B*) Confocal immunofluorescence microscopy on sagittal sections of wild-type (WT) cerebellum (*left* panel), L7-Cre DKO cerebellum at P20 (*middle* panel), and L7-Cre DKO cerebellum at P70 (*right* panel). (*A*) Overlayed images of sections probed for Rbfox1 (green) and Rbfox2 (red) expression. (*B*) Overlayed Z-stack projections of sections probed for Calbindin (green), counterstained with DAPI (blue). (ML) Molecular layer; (PCL) Purkinje cell layer; (iGCL) internal granule cell layer. Bars, 50 μm. (*C*) Quantification of wild-type and L7-DKO performance on the rotarod test; error bars represent SEM. Statistical significance was calculated by Wilcoxon rank sum test (nonparametric). (**) $P = 0.0032$; (*n.s.*) not significantly different between wild type and L7-DKO. $n = 27$ wild-type and 25 L7-DKO animals.

Using the rotarod behavioral assay, we quantitatively assessed the motor function of the L7-DKO mice at age P70. On the first rotarod trial, adult mutant mice showed a mean latency to fall that was significantly shorter ($P = 0.0032$) than wild-type animals (Fig. 4C). Performance of the wild-type littermate controls distinctly improved with motor learning over the next three consecutive rotarod trials, although the variability in their performance also increased, presumably due to variation in their genetic background. In contrast, performance improved only slightly with each trial for the L7-DKO mice, and the L7-DKO mice were clearly deficient in function relative to wild type. In tests of other behaviors, such as the open field test used to assess anxiety and exploratory behavior, L7-DKO mice showed no deviation from wild type (data not shown). There was also no statistically significant difference in rotarod performance between L7-DKO males and L7-DKO females. Thus, although other neurological functions remain intact, the L7-DKO mice are impaired for motor function.

To assess their possible physiological deficits, we performed electrophysiological recording of Purkinje cells in the various Rbfox mutant mouse strains. Normal Purkinje cells exhibit spontaneous and regular firing of pacemaking action potentials (Hausser and Clark 1997). Because of their more severe phenotype, we first examined mice carrying *Nestin-Cre*. Using extracellular recording, we measured the spontaneous firing of Purkinje cells in cerebellar slices of wild-type, $Rbfox2^{-/-}$, and $Rbfox1^{+/-}/Rbfox2^{-/-}$ mice. Representative traces from single Purkinje cells from each of these three genotypes are shown in Figure 5A. Compared with wild-type cells, $Rbfox2^{-/-}$ Purkinje cells exhibit a moderate decrease in firing frequency, while $Rbfox1^{+/-}/Rbfox2^{-/-}$ Purkinje cells show a dramatically decreased frequency (Fig. 5B). Strikingly, the firing of both $Rbfox2^{-/-}$ and $Rbfox1^{+/-}/Rbfox2^{-/-}$ cells is highly irregular, as indicated by a large coefficient of variation in their interspike interval (ISI). Thus, both Rbfox2 and Rbfox1 contribute to Purkinje cell pacemaking (Fig. 5B).

To examine the requirement for the Rbfox proteins in mature Purkinje cells, we also recorded their firing in L7-DKO cerebellar slices. Representative traces from wild-type and L7-DKO Purkinje cells at P20 and at P70 are shown in Figure 5C. At age P20, L7-DKO Purkinje cells showed a firing frequency and coefficient of variation unchanged from that of wild-type Purkinje cells (Fig. 5D). In contrast, by P70, firing frequency in L7-DKO Purkinje cells declined by 60% (Fig. 5D). The regularity of firing was even more dramatically affected, with a 13-fold increase in the ISI coefficient of variation, very similar to the defect seen in $Rbfox2^{+/-}/Rbfox2^{-/-}$ slices. The more severe deficit in firing frequency observed in $Rbfox1^{+/-}/Rbfox2^{-/-}$ Purkinje cells may be due to developmental

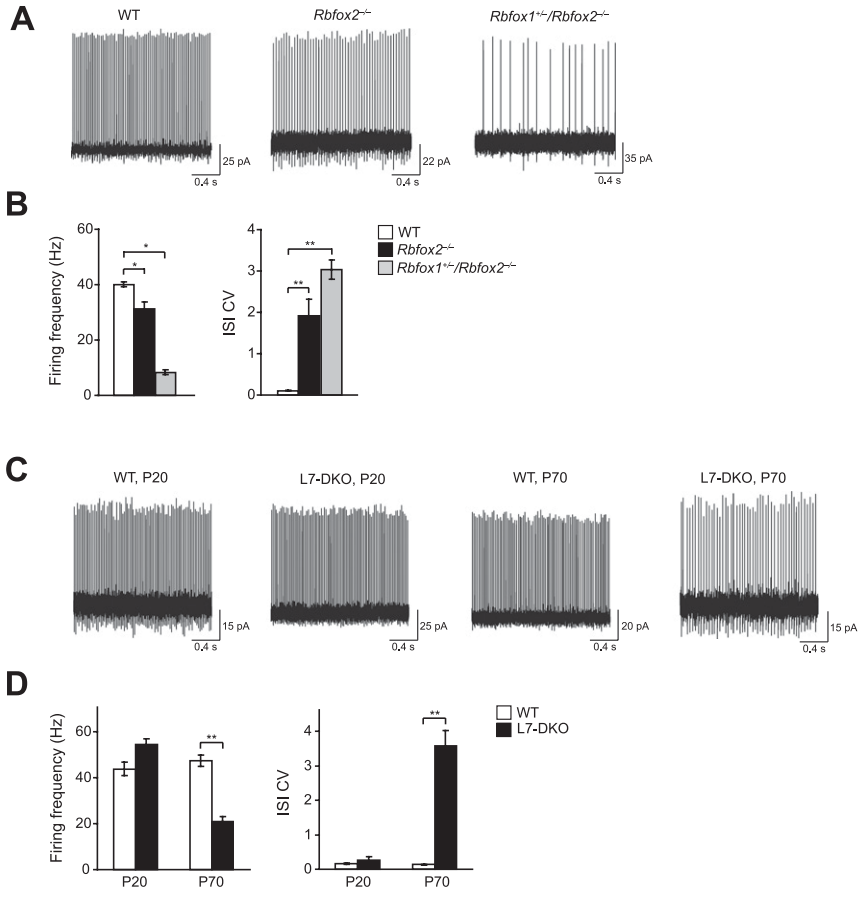

Figure 5. $Rbfox1^{+/loxP}/Rbfox2^{loxP/loxP}/Nestin\text{-}Cre^{+/-}$ and L7-DKO mice show highly irregular Purkinje cell electrophysiology. (*A*) Representative contiguous segments of an extracellular recording from a single Purkinje cell (PC) in the various *Rbfox*/*Nestin* knockouts. (*B*) Pooled data for Purkinje cell mean firing frequency and coefficient of variation of interspike intervals (ISI CV) in the various *Rbfox*/*Nestin* knockouts. n = 99, 89, 100, and 139 cells for wild type (WT), $Rbfox2^{-/-}$, $Rbfox1^{-/-}/Rbfox2^{+/-}$, and $Rbfo1^{+/-}/Rbfox2^{-/-}$, respectively. (*C*) Representative contiguous segments of an extracellular recording from a single Purkinje cell in wild-type and L7-DKO mice at age P20 or P70. (*D*) Pooled data for Purkinje cell mean firing frequency and ISI CV in wild-type and L7-DKO mice. n = 43, 63, 39, and 71 cells for wild-type P20, L7-DKO P20, wild-type P70, and L7-DKO P70, respectively. Error bars, SEM. Statistical significance was calculated by ANOVA testing, followed by post-hoc Tukey paired comparisons with Bonferroni correction for multiple comparisons. (*) $P < 0.005$; (**) $P < 2 \times 10^{-6}$.

defects resulting from the earlier gene deletion or may be attributed to the loss of Rbfox proteins in additional cell types. These results demonstrate that Rbfox-mediated splicing regulation is required in mature neural circuits and not just in the developing brain. In particular, Rbfox proteins are required for proper Purkinje cell pacemaking.

The $Na_v1.6$ sodium channel transcript requires Rbfox proteins for proper cerebellar expression

Regular spontaneous firing of Purkinje cells is in part mediated by a resurgent current from sodium channels that promotes rapid recovery from an inactivated to an open channel state (Raman and Bean 1997). The voltage-gated sodium channel α subunit $Na_v1.6$ (*Scn8a*), along with a β4 accessory subunit (*Scn4b*), is required for the resurgent sodium current in Purkinje cells (Raman et al. 1997; Grieco et al. 2005). L7-Scn8a-KO mice that lack the $Na_v1.6$ channel in Purkinje cells exhibit impaired rotarod performance and reduced spontaneous firing, very similar to the L7-DKO mice (Raman et al. 1997; Meisler et al. 2001; Levin et al. 2006).

The Scn8a transcript contains two pairs of mutually exclusive exons. Exons 5N and 5A encode alternative versions of transmembrane segments S3 to S4 within domain I of the channel, and exons 18N and 18A encode similar alternative versions of segments S3 to S4 within domain III. The different domain I sequences encoded by exons 5N and 5A could influence either its voltage-dependent gating or its interaction with the blocking subunit β4 that is important for the resurgent sodium current (Grieco et al. 2005). In domain III, exon 18A encodes the full S3-to-S4 segment. However, Exon 18N contains a conserved in-frame stop codon that prematurely truncates the reading frame, leading to nonsense-mediated mRNA decay (Plummer et al. 1997; O'Brien et al. 2011). Still another mRNA isoform, the Δ18 transcript, maintains the original reading frame, but lacks segments S3 and S4 of domain III altogether. Thus, exon 18A splicing is likely required to produce a functional channel.

These exons are regulated developmentally, with transcripts containing exons 5N and 18N predominant in the embryonic brain and exons 5A and 18A transcripts more abundant in the adult (Plummer et al. 1997). Potential Rbfox-binding motifs are present downstream from both exons 5A and 18A (Fig. 6A,C). Moreover, exon 18A has been shown to be activated by ectopically expressed Fox proteins. This enhancement is dependent on the first downstream UGCAUG element, which is conserved in vertebrates (O'Brien et al. 2011). As predicted, exon 5A splicing is moderately decreased in *Rbfox2*$^{-/-}$ and *Rbfox1*$^{-/-}$ whole-brain RNA (Table 1; Gehman et al. 2011) and in the cerebellum (Fig. 6B). Notably, in the *Rbfox1*$^{+/-}$/*Rbfox2*$^{-/-}$ cerebellum, exon 5A splicing is much more strongly affected than in either single knockout (Fig. 6B). Exon 18A shows a dramatic change in the *Rbfox1*$^{+/-}$/*Rbfox2*$^{-/-}$ cerebellum (Fig. 6D). Splicing of this exon changes little in the *Rbfox1*$^{-/-}$ cerebellum and shows only a modest decrease with the loss of Rbfox2. In the *Rbfox1*$^{+/-}$/*Rbfox2*$^{-/-}$ cerebellum, exon 18A inclusion decreases from >80% to <40%. This is accompanied by a concurrent increase in the 18N embryonic isoform, as well as the double exon-skipped (Δ18) isoform. At the protein level, expression of the ~225-kDA $Na_v1.6$ channel is reduced by 50% in the *Rbfox1*$^{+/-}$/*Rbfox2*$^{-/-}$ cerebellum compared with wild type. We did not detect bands of lower molecular weight that might correspond to truncated $Na_v1.6$ isoforms (Fig. 6E). These isoforms may lack the epitope targeted by the antibody or may be unstable, as it is not unusual for spliced isoforms leading to nonsense-mediated decay to produce little observable product (Boutz et al. 2007; McGlincy et al. 2010; Sun et al. 2010; Zheng et al. 2012). Since the Purkinje cell-specific loss of Scn8a produces a similar pacemaking defect, the substantial reduction in $Na_v1.6$ sodium channel due to the altered splicing of the Scn8a transcript is presumably one component of the aberrant Purkinje cell firing in the *Rbfox1*$^{+/-}$/*Rbfox2*$^{-/-}$ cerebellum. However, there are changes in the splicing of other transcripts affecting membrane physiology and calcium homeostasis in these mice, and it is likely that other deficits also contribute to the firing phenotype. Clearly, one function of the Rbfox1 and Rbfox2 post-transcriptional regulatory program is to control $Na_v1.6$ expression and allow proper Purkinje cell pacemaking.

Discussion

Rbfox2 is needed for cerebellar development

We found that the Rbfox RNA-binding proteins are essential for both the proper development and the mature physiology of the cerebellum. Purkinje cells develop relatively early in embryonic development and are largely in place by birth, before the development of most other cerebellar cells. The migration and differentiation of these cells is controlled by a variety of transcription factors and signaling pathways, including Math1, BDNF, and Reelin (Wang and Zoghbi 2001). We found that post-transcriptional regulatory processes also play a key role in these events.

The regulatory network controlled by Rbfox2 is large and will make diverse contributions to Purkinje cell biology. Rbfox2 deficiency early in brain development results in reduced cerebellar size and a neuronal migration phenotype with ectopic Purkinje cells, similar to defects observed from Reelin signaling mutations (Fig. 2C–E). Defects in Reelin signaling generally affect migration of both cortical and Purkinje neurons. Another splicing factor, Nova2, has been shown to regulate cortical neuron and Purkinje cell migration by altering the splicing of the Reelin signaling adaptor Dab1 (Yano et al. 2010). We did not observe changes in Dab1 splicing in the Rbfox2 brain. Also, the *Rbfox2*$^{-/-}$ brain shows primarily defects in Purkinje cell migration and not in cortical layering. During the period of their migration, Rbfox2 is the only Rbfox family member expressed in Purkinje cells, whereas in much of the CNS, it is typically coexpressed with the Rbfox1 and Rbfox3 proteins. Thus, the lack of a phenotype in parts of the Rbfox2 knockout brain may be due to Rbfox1 and Rbfox3 compensating for the loss of Rbfox2. It

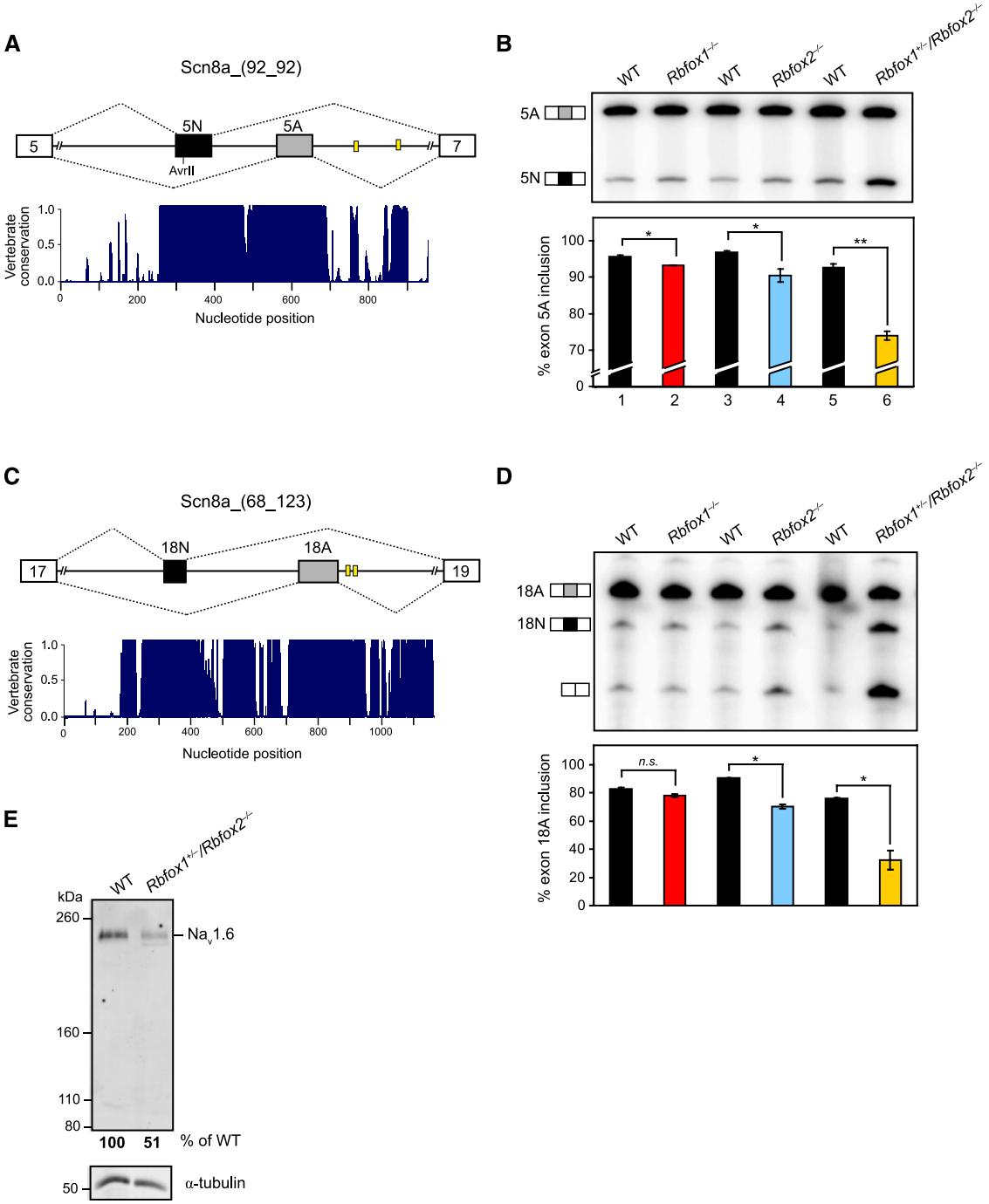

Figure 6. The *Rbfox1*$^{+/-}$/*Rbfox2*$^{-/-}$ cerebellum exhibits strong changes in splicing of two pairs of mutually exclusive exons of Scn8a, the transcript encoding the $Na_v1.6$ sodium channel. (*A*,*C*) Schematics showing the two pairs of Scn8a mutually exclusive exons, 5N/5A (*A*) and 18N/18A (*C*); horizontal black bars represent the upstream "N" (neonatal) exon, and horizontal gray bars represent the downstream "A" (adult) exon. Thin horizontal lines represent the intervening intron and the promixal 300 nt of the adjacent introns. Yellow boxes represent (U)GCAUG motifs. A histogram displaying the degree of conservation of this region among 30 vertebrate species, as determined by phastCons, is shown *below* each schematic. A score of 1 indicates 100% identity among all species at that nucleotide position. A distance scale in nucleotides is shown *below* the histogram. (*B*,*D*) Denaturing gel electrophoresis of Scn8a 5N/5A (*B*) and 18N/18A (*D*) RT–PCR products in cerebellar samples from mice of the listed genotypes. The exon A-included and exon N-included bands are indicated. Graphs of the mean inclusion percentage of exons 5A and 18A are shown *below* the gels. Error bars, SEM; $n = 3$. (*) $P < 0.05$; (**) $P < 0.005$ by paired, one-tailed Student's *t*-test. (*E*) Immunoblot analysis of $Na_v1.6$ protein in membrane fractions isolated from wild-type and *Rbfox1*$^{+/-}$/*Rbfox2*$^{-/-}$ cerebelli. α-Tubulin was used as a loading control for total membrane protein. *Below* the gel is the amount of $Na_v1.6$ protein in each sample as a percentage of wild type, normalized by α-tubulin expression.

will be interesting to assess Lrp8 splicing specifically in nascent Purkinje cells rather than in the whole brain (Koch et al. 2002) and determine the contribution of the change in Lrp8 to the neuronal migration phenotype. This will require a Cre line that expresses the recombinase much earlier than L7-Cre. Moreover, additional Rbfox2 targets are also likely to contribute to the developmental phenotype of the *Rbfox2*$^{-/-}$ mice.

We found that Rbfox1 and Rbfox2 have both common and differential functions. The different mutant phenotypes resulting from their CNS-specific deletion indicate that the Rbfox proteins are not truly redundant. In contrast to the cerebellar phenotype seen in *Rbfox2*$^{-/-}$ mice, the *Rbfox1*$^{-/-}$ brain exhibits largely normal development but is prone to seizures (Gehman et al. 2011). The early phenotype of the *Rbfox2*$^{-/-}$ mice was expected from its earlier expression compared with Rbfox1. However, even in the adult, there are exons whose splicing appears more sensitive to one Rbfox protein or the other. The unique target exons for each Rbfox protein may result in part from their temporal- and spatial-specific patterns of expression and in part from differences in their protein–protein interactions and cooperation with other factors on particular transcripts.

There is also clearly some functional redundancy between Rbfox1 and Rbfox2. The two proteins have identical RNA-binding domains and highly overlapping expression patterns in the brain, and *Rbfox1*$^{-/-}$ and *Rbfox2*$^{-/-}$ brains exhibit some splicing changes in common. In keeping with these common targets, CNS-specific double deletion of both Rbfox1 and Rbfox2 results in perinatal lethality, indicating that at least one copy of these proteins is required for proper brain development. Mice heterozygous for Rbfox1 and null for Rbfox2 (*Rbfox1*$^{+/loxP}$/*Rbfox2*$^{loxP/loxP}$/*Nestin-Cre*$^{+/-}$) have a reduced cerebellum, similar to the single Rbfox2 knockout (*Rbfox2*$^{loxP/loxP}$/*Nestin-Cre*$^{+/-}$). However, they exhibit a more severe ataxia as well as more pronounced defects in Purkinje cell firing (Fig. 5A,B; Supplemental Movie 1). For some targets, it appears that the double knockout results in a more severe alteration in splicing than either single mutation alone.

Rbfox proteins are required for Purkinje cell pacemaking

To examine the contribution of Rbfox proteins to the function of mature neurons after proper development, we created mice with Purkinje cell-specific double deletion of Rbfox1 and Rbfox2 (L7-DKO). These mice did not show developmental brain defects, but adult L7-DKO mice exhibited highly irregular Purkinje cell firing (Fig. 5C,D) and impaired motor function (Fig. 4C). Thus, the Rbfox proteins are required in adult Purkinje cells. The ataxia and irregular Purkinje cell firing of *Rbfox1*$^{+/loxP}$/*Rbfox2*$^{loxP/loxP}$/*Nestin-Cre*$^{+/-}$ mice are at least in part a Purkinje cell-intrinsic phenotype.

The spontaneous firing of Purkinje cells depends on sodium currents mediated by the voltage-gated sodium channel α subunit $Na_v1.6$ (*Scn8a*). Knockout of *Scn8a* expression in Purkinje cells with L7-Cre results in impaired motor function similar to that in the L7-DKO mice (Levin et al. 2006). This sodium channel is subject to rapid blockade by the associated β4 (*Scn4b*) subunit, which binds open channels upon depolarization and is released upon repolarization to produce a resurgent sodium current (Grieco et al. 2005). Binding of the β4 subunit blocks the channel and limits classical inactivation of $Na_v1.6$. Rapid detachment of β4 at hyperpolarized potentials then leaves the channel transiently open, providing a pacemaking "drive" current, which is required for rapid firing (Raman et al. 1997; Grieco et al. 2005). The *Rbfox1*$^{+/-}$/*Rbfox2*$^{-/-}$ cerebellum exhibits altered splicing of two pairs of mutually exclusive Scn8a exons, 5A/5N and 18A/18N. The increased expression of the embryonic/neonatal Scn8a transcripts in these mice leads to reduced $Na_v1.6$ protein (Fig. 6B,D). Thus, through their control of Scn8a splicing, the Rbfox proteins are required for the development and maintenance of proper Purkinje cell physiology. It will be very interesting to examine how this control affects Scn8a expression and Purkinje cell function in developing and mature cerebellar circuits as different Rbfox proteins come into play and are themselves dynamically regulated (Lee et al. 2009).

Studies of both human neurological disease mutations and mouse models have linked Rbfox proteins to epilepsy, ataxia, and autism spectrum disorder (Bhalla et al. 2004; Barnby et al. 2005; Martin et al. 2007; Sebat et al. 2007; Voineagu et al. 2011). We found that the diverse spliced isoforms whose production is dependent on Rbfox are important for both establishing and maintaining proper neuronal circuits. The post-transcriptional regulatory networks controlled by these proteins are extensive, and like other splicing factor mutations, the loss of either Rbfox1 or Rbfox2 has highly pleiotropic effects (Jensen et al. 2000; Wang et al. 2001; Kanadia et al. 2003; Ule et al. 2005; Xu et al. 2005). Confronting this pleiotropy will be essential in understanding the roles of these factors in neurological disease.

Materials and methods

Mice

We used homologous recombination to create "floxed" Rbfox2 alleles consisting of *loxP* sites flanking *Rbfox2* exons 6 and 7, annotated as previously described (Damianov and Black 2010). Southern blot hybridization probes were generated by PCR amplification and cloned using TOPO TA cloning kit (Invitrogen). The probes were cut out of the TOPO vectors using EcoRI and labeled by PCR in the presence of α-^{32}PdCTP. Mouse strain 129S6/SVEvTac BAC library (RPCI-22), arrayed on high-density nylon filters, was obtained from Children's Hospital Oakland Research Institute (CHORI). Probe Fox2-BAC was used to screen the BAC library. Positive clones were purchased from CHORI and validated by PCR with the primers used in generating Probe 1 and Probe 2. Clone RP22-317J11 was used as templates to amplify the fragments between the BamHI sites (Supplemental Fig. 1). The upstream arm and the targeted sequence were amplified using primers Fox2-knpr-F and Fox2-mid-R. The downstream arm was amplified using primers Fox2-right-F and Fox2-PRB2-R. The upstream and downstream arms were digested with BamHI, blunted with Klenow, and cloned in the XbaI and SalI sites

of pFlox-PGK-Neo. The fragment containing exons 6 and 7 was inserted in the BamHI site between the two *loxP* sites. The primers used for the construction of the targeting cassette and the generation of hybridization probes are as follows: Fox 2 BAC: Fox2-bac-F (5′-GGCCCTAAGTTTGGTTCCTC-3′) and Fox2-bac-R (5′-GCAAGGCAAGCTGGTTTAAG-3′); Probe 1 (upstream probe): Fox2-knpr-R (5′-CTAAAGGGCAGCCATCACTC-3′) and Fox2-knpr-F (5′-TGATGATTTATTTTAGATTAGCCCAAG-3′); Probe 2 (downstream probe): Fox2-PRB2-F (5′-AATCCCATG CATTCCATCAT-3′) and Fox2-PRB2-R (5′-AATGCTTCTGG GTGGAAATG-3′); targeting cassette cloning: Fox2-right-F (5′-TCTGCTCACCTGTCTCACCTCC-3′) and Fox2-mid-R (5′-CTCATCCTGGATCCTCTGAAAGATCAGTT-3′). The targeting cassette was transfected into 129S2/Sv ESCs at the University of California at Los Angeles (UCLA) ESC core facility. Clones that had undergone homologous recombination were identified by Southern blot using Probes 1 and 2 after digesting the genomic DNA with XmaI. The Neo/TK selection cassette was removed by electroporation of Cre-expressing plasmid (pTurbo-Cre) and ganciclovir selection at the UCLA ESC core. The deletion of the selection cassette was confirmed by Southern blot with Probes 1 and 2. Cells from positive clones were injected into C57BL/6J blastocysts at the University of California at San Diego transgenic and gene targeting core, and one line was found to have germline transmission. Heterozygous (*Rbfox2*$^{loxP/+}$) F1 offspring were crossed, and the resulting homozygous (*Rbfox2*$^{loxP/loxP}$) mice were crossed to transgenic *Nestin-Cre*$^{+/-}$ mice. Resulting heterozygotes (*Rbfox2*$^{loxP/+}$/*Nestin-Cre*$^{+/-}$) were crossed to *Rbfox2*$^{loxP/loxP}$ mice to obtain homozygous (*Rbfox2*$^{loxP/loxP}$/*Nestin-Cre*$^{+/-}$) offspring. Genotyping for the *Rbfox2*$^{+}$ and *Rbfox2*^{loxP} alleles was performed by PCR using primers Rbfox2-Mid-F (5′-CAGAAA CAAGAAAGGCCTCACTTCAG-3′) and Rbfox2-Scr-R (5′-CTC TGACTTATACATGCACCTC-3′) with standard PCR conditions, resulting in a 320-base-pair (bp) wild-type and a 453-bp *Rbfox2*^{loxP} PCR product. The *Rbfox2*$^{\Delta}$ allele was genotyped in DNA extracted from brain tissue using the above Rbfox2-Scr-R primer plus the primer Rbfox2-Seq-LM-F (5′-GATGGGGTTTTATATG TGGAG-3′) with a product of 350 bp; the nondeleted allele is too large to be amplified with these primers. The presence of *Nestin-Cre* was evaluated using primers Nes-For (5′-CGTGTTGCACT GAACGCTAA-3′) and Cre-Rev (5′-GCAAACGGACAGAAGCA TTT-3′), resulting in a PCR product of 470 bp. Mice used for this study were maintained on a mixed 129S2/Sv × C57BL/6J background. Animals were housed in a 12-h light/dark cycle with food and water available ad libitum and were maintained by the UCLA Association for Assessment and Accreditation of Laboratory Animal Care accredited Division of Laboratory Medicine. All experiments were Institutional Animal Care and Use Committee-approved by the UCLA Chancellor's Animal Research Council.

Histology and immunohistochemistry

For animals aged P14 and above, *Rbfox2*$^{loxP/loxP}$/*Nestin-Cre*$^{+/-}$ and wild-type littermates were transcardially perfused with ice-cold 0.1 M phosphate-buffered saline (PBS; pH 7.4), followed by ice-cold 4% paraformaldehyde (PFA) in PBS (pH 7.4). Brains were cryoprotected in 30% sucrose, 40-μm free-floating sections were cut in the sagittal orientation using a cryostat, and sections were stored at −80°C until use. For animals younger than P14, brains from *Rbfox2*$^{loxP/loxP}$/*Nestin-Cre*$^{+/-}$ and wild-type littermates were fixed in PFA for 24 h and embedded in paraffin, and 5-μm sections were cut in the sagittal orientation using a microtome. Prior to use, paraffin-embedded sections were deparaffinized with xylenes and rehydrated, and antigens were unmasked using 0.01 M sodium citrate solution at 95°C. For Nissl histology, 40-μm cerebellar sections were thawed, hydrated, and stained using 0.25% thionin acetate (Sigma); dehydrated through alcohols and xylenes; and mounted with DPX (Electron Microscopy Sciences). For double immunofluorescent staining, 5-μm and 40-μm brain sections were blocked for 30 min with blocking solution (10% normal goat serum, 0.1% Triton X-100 in PBS) and incubated with primary antibodies diluted in blocking solution overnight at 4°C. Sections were washed three times with 0.1% Triton X-100 in PBS and stained with secondary antibodies in PBS for 2 h. Sections were again washed three times with 0.1% Triton X-100 in PBS, mounted with ProLong Gold plus DAPI reagent (Invitrogen), and imaged using a Zeiss LSM 510 Meta confocal microscope. Z-stack projections of Purkinje cells (Fig. 4B) were calculated from five 2.2-μm-thick Z sections per region. The following primary antibodies were used: mouse α-Rbfox1 1D10, 1:200; rabbit α-Rbfox2, 1:200 (Bethyl Laboratories); rabbit α-Calbindin D-28K, 1:800 (Millipore); mouse α-NeuN, 1:800 (Millipore). Alexa Fluor 488-conjugated goat α-mouse IgG, Alexa Fluor 568-conjugated goat α-rabbit IgG secondary antibodies, and Alexa Fluor 598-conjugated streptavidin (Molecular Probes) were used at 1:1000. Histological staining and immunostaining shown are representative of at least two independent samples. TUNEL staining was performed using the NeuroTACS II In Situ Apoptosis Detection kit (Trevigen) according to the manufacturer's instructions. To calculate the number of TUNEL-positive cells (Fig. 2E) and the total number of ectopic and nonectopic Purkinje cells (Supplemental Fig. 2A,B), three sections nearest the midline from three animals of each genotype were used. Area measurements were calculated using ImageJ. Data were analyzed by paired, one-tailed Student's *t*-test, and $P < 0.05$ was defined as significant.

Western blotting

Nuclei were isolated from wild-type, *Rbfox2*$^{+/-}$, and *Rbfox2*$^{-/-}$ brains as previously described (Grabowski 2005). Nuclei were lysed in lysis buffer (20 mM Hepes-KOH at pH 7.9, 300 mM NaCl, 1 mM EDTA, 0.75% NP-40) containing complete protease inhibitors (Roche) for 10 min on ice. The lysates were cleared by centrifugation at 20,000*g* for 15 min and boiled for 5 min in SDS loading buffer. Proteins were resolved on 10% Tris-glycine gels. For preparation of membrane fractions, cerebelli from three mice aged P21 were pooled for each genotype, homogenized in RIPA buffer, and pelleted at 100,000*g* for 30 min at 4°C. Pellets were resuspended in buffer (50 mM Tris, 2 mM $CaCl_2$, 80 mM NaCl, 1% Triton X-100) and spun at 100,000*g* for 30 min at 4°C. Supernatants were collected and diluted in SDS loading buffer, and proteins were resolved on 6% Tris-glycine gels. Antibodies were used at the following dilutions: α-Rbfox1 1D10, 1:2000; α-Rbfox2, 1:2000 (Bethyl Laboratories); α-U1-70K, 1:5000; α-$Na_v1.6$, 1:200 (AbCam); α-α-tubulin, 1:1000 (Calbiochem); ECL Plex Cy3-conjugated goat α-mouse and Cy5-conjugated goat α-rabbit secondary antibodies, 1:2500 (GE Healthcare). Blots were scanned in a Typhoon 9400 PhosphorImager scanner (GE Healthcare), and images were quantified and analyzed with ImageQuant TL software.

ML width and BrdU proliferation assays

BrdU (Sigma) was used to identify cells in S phase. Two animals of each genotype were injected i.p. with BrdU (100 μg per gram body weight) on P7. Two hours or 72 h later, the mice were sacrificed, and the brains were immersed in 4% PFA overnight at 4°C. Brains were snap-frozen, embedded in Tissue-Tek (Sakura), and cut into 20-μm-thick sagittal sections on a cryostat (Leica). Sections were incubated in 2× SSC (0.3 M NaCl, 0.03 M sodium citrate) plus 50% formamide for 2 h at 65°C. Sections were rinsed

in 2× SSC and incubated in 2 M HCl for 30 min at 37°C. Slides were washed in 0.1 M boric acid (pH 8.5) for 10 min and processed for immunofluorescent staining as above. The following primary antibodies were used: mouse α-BrdU PRB-1, 1:250 (Invitrogen); rabbit α-Calbindin D-28K, 1:800 (Millipore); mouse α-NeuN, 1:800 (Millipore). Alexa Fluor 488-conjugated goat α-mouse IgG and Alexa Fluor 568-conjugated goat α-rabbit IgG secondary antibodies (Molecular Probes) were used at 1:1000. Quantifications were performed on three sections nearest the midline, in three different cerebellar lobes (III, VI, and IX). For measuring the length of the ML, five length measurements per lobe per section were made, and the mean length in microns for each lobe was calculated. For BrdU quantification at 2 h, the length of the eGCL in microns was measured, and the number of cells located in this length and expressing BrdU were counted. The number of $BrdU^+$ cells was divided by the length of the eGCL. For BrdU quantification at 72 h, the total area of the ML and the iGCL in square microns were measured, and the $BrdU^+$ cells in this area were counted. The number of $BrdU^+$ cells was divided by the total area.

Splicing microarrays

Total RNA was extracted by Trizol reagent (Invitrogen) from the whole brains of three wild-type and three *Rbfox2*$^{loxP/loxP}$/*Nestin-Cre*$^{+/-}$ mice, all 1-mo-old males. Ribosomal RNAs were removed from the samples using the RiboMinus Transcriptome Isolation kit (Invitrogen) according to the manufacturer's instructions. Amplified, biotinylated cDNA target was produced using the GeneChip Whole Transcript Sense Target Labeling and Control Reagents kit (Affymetrix) according to the manufacturer's instructions. Each sample target was hybridized overnight to a Mouse GeneSplice Array (Affymetrix, PN 540092). Hybridized arrays were processed using the Affymetrix Fluidics Station 450 and scanned with an Affymetrix GeneChip scanner. Data were analyzed, and each alternative event was assigned a separation score (sepscore or MJAY ratio), a measure of the difference in the average ratio of inclusion to skipping for the indicated exon in the *Rbfox2*$^{-/-}$ samples compared with wild type, as previously described (Sugnet et al. 2006). Of the top 26 splicing changes identified on the array, 21 were confirmed by RT–PCR, representing an 81% validation rate. To assess enrichment of (U)GCAUG elements in the exons identified as changing in the mutant mice, we measured the frequency of putative Rbfox-binding elements adjacent to all exons probed on the MJAY array. Of the 5166 alternative cassette exons probed by the array, only 1590 (31%) possess a (U)GCAUG motif within 300 nt downstream, and only 1328 (26%) possess this motif within 300 nt upstream. In contrast, 80% of the exons changing in the *Rbfox2*$^{-/-}$ brain carry adjacent (U)GCAUG motifs, and many have multiple motifs.

RT–PCR assays

Total RNA was extracted by Trizol reagent (Invitrogen) from the whole brains of 1-mo-old wild-type and *Rbfox2*$^{loxP/loxP}$/*Nestin-Cre*$^{+/-}$ mice (n = 3 for each genotype). One microgram of total RNA was reverse-transcribed with random hexamers. One-tenth of this reaction was then amplified in 24 cycles of PCR with exon-specific primers, one of which was ^{32}P-labeled. The PCR products were resolved on 8% polyacrylamide/7.5 M urea denaturing gels. The gel was dried, exposed, and scanned in a Typhoon 9400 PhosphorImager scanner (GE Healthcare). Images were analyzed with ImageQuant TL software. Primers used for assaying each exon are listed in Supplemental Table 1. For Figure 6, total RNA was extracted from the cerebelli of 1-mo-old *Rbfox1*$^{loxP/loxP}$/*Nestin-Cre*$^{+/-}$ mice, *Rbfox2*$^{loxP/loxP}$/*Nestin-Cre*$^{+/-}$ mice, or *Rbfox1*$^{+/loxP}$/*Rbfox2*$^{loxP/loxP}$/*Nestin-Cre*$^{+/-}$ mice plus wild-type littermates (n = 3 for each genotype), and the RT–PCR assay was performed in the same manner as described above.

Behavioral testing

For analyzing balance and motor coordination, 27 wild-type and 25 L7-DKO mice of both sexes (2–3 mo) were tested on the automated accelerating rotarod (RotoRod 3375-5, TSE Systems). The rotational speed increased from 5 to 20 rpm over 10 sec. Mice were acclimated to the rotarod for 3 min, then tested on four trials with a 1-h rest period between each trial. The latency to fall from the rotarod was recorded, with a timeout (maximum period) of 180 sec. Mean values for each of the four trials were calculated for each genotype. The Wilcoxon rank sum test was used to assess statistical significance of differences in the latency to fall for each trial. In all cases, $P < 0.05$ was considered statistically significant.

Electrophysiology

In general, tissue preparation and recording methods were identical to those described in prior studies (Smith and Otis 2005). To obtain cerebellar slices, transgenic and wild-type mice of the indicated ages were anesthetized with isofluorane and decapitated. The brains were quickly removed and placed in cold extracellular solution containing 119 mM NaCl, 2.5 mM KCl, 2.5 mM $CaCl_2$, 1.3 mM $MgCl_2$, 1 mM NaH_2PO_4, 26 mM $NaHCO_3$, and 11 mM glucose (pH 7.4) when gassed with 5% CO_2/95% O_2. Parasaggital slices were made after dissecting the cerebellum using a vibratome (Leica VT1000). The slices were kept in oxygenated extracellular solution for 30 min at 35°C, and then at room temperature until use (1–5 h). For extracellular recordings, slices were placed in a recording chamber on the stage of an upright microscope and superfused with the extracellular recording solution maintained at 32.5°C–34.5°C. Purkinje cells were visually identified using a 40× water immersion objective. Borosilicate glass pipettes (World Precision Instruments) with 1–3 MΩ resistance when filled with extracellular solution were placed near the soma/axon initial segment in order to record AP-associated capacitive current transients with the extracellular pipette voltage held at 0 mV. Recordings were amplified/digitized by an Axon amplifier/interface (multiclamp 700 B or 200 B and Digidata 1440). For analysis, spike detection was accomplished using Pclamp 10 software, and subsequent analysis was performed in Excel and Igor. Figures were made in Igor (Fig. 5A,C). Data are displayed as mean ± SEM (Fig. 5B,D). Statistical significance was calculated using ANOVA testing followed by post-hoc Tukey paired comparisons with Bonferroni correction for multiple comparisons.

Acknowledgments

This work was done in collaboration with X.-D. Fu (University of California at San Diego). We thank N. Copeland (Institute of Molecular and Cell Biology, Singapore) for the recombineering vectors and bacterial strains used for generating the transgenic Rbfox2 mice, and J.P. Donahue for his help with the microarray analyses. K. Martin gave us helpful comments on the manuscript. This work was supported in part by US National Institutes of Health Grants R01 GM049369 to X.D.F., R01 GM084317 to M.A. and D.L.B., R01 GM49662 to D.L.B, and R01 86429 to T.S.O. D.L.B. is an Investigator of the Howard Hughes Medical Institute. T.S.O. and P.M. are supported by grants from NINDS and the McKnight Foundation.

References

Auweter SD, Fasan R, Reymond L, Underwood JG, Black DL, Pitsch S, Allain FH. 2006. Molecular basis of RNA recognition by the human alternative splicing factor Fox-1. *EMBO J* **25:** 163–173.

Baraniak AP, Chen JR, Garcia-Blanco MA. 2006. Fox-2 mediates epithelial cell-specific fibroblast growth factor receptor 2 exon choice. *Mol Cell Biol* **26:** 1209–1222.

Barnby G, Abbott A, Sykes N, Morris A, Weeks DE, Mott R, Lamb J, Bailey AJ, Monaco AP. 2005. Candidate-gene screening and association analysis at the autism-susceptibility locus on chromosome 16p: Evidence of association at GRIN2A and ABAT. *Am J Hum Genet* **76:** 950–966.

Barski JJ, Dethleffsen K, Meyer M. 2000. Cre recombinase expression in cerebellar Purkinje cells. *Genesis* **28:** 93–98.

Bhalla K, Phillips HA, Crawford J, McKenzie OL, Mulley JC, Eyre H, Gardner AE, Kremmidiotis G, Callen DF. 2004. The de novo chromosome 16 translocations of two patients with abnormal phenotypes (mental retardation and epilepsy) disrupt the A2BP1 gene. *J Hum Genet* **49:** 308–311.

Black DL. 2003. Mechanisms of alternative pre-messenger RNA splicing. *Annu Rev Biochem* **72:** 291–336.

Blencowe BJ. 2006. Alternative splicing: New insights from global analyses. *Cell* **126:** 37–47.

Boutz PL, Stoilov P, Li Q, Lin CH, Chawla G, Ostrow K, Shiue L, Ares M Jr, Black DL. 2007. A post-transcriptional regulatory switch in polypyrimidine tract-binding proteins reprograms alternative splicing in developing neurons. *Genes Dev* **21:** 1636–1652.

Calarco JA, Superina S, O'Hanlon D, Gabut M, Raj B, Pan Q, Skalska U, Clarke L, Gelinas D, van der Kooy D, et al. 2009. Regulation of vertebrate nervous system alternative splicing and development by an SR-related protein. *Cell* **138:** 898–910.

Chen M, Manley JL. 2009. Mechanisms of alternative splicing regulation: Insights from molecular and genomics approaches. *Nat Rev Mol Cell Biol* **10:** 741–754.

Cooper TA, Wan L, Dreyfuss G. 2009. RNA and disease. *Cell* **136:** 777–793.

Damianov A, Black DL. 2010. Autoregulation of Fox protein expression to produce dominant negative splicing factors. *RNA* **16:** 405–416.

Faustino NA, Cooper TA. 2003. Pre-mRNA splicing and human disease. *Genes Dev* **17:** 419–437.

Gehman LT, Stoilov P, Maguire J, Damianov A, Lin CH, Shiue L, Ares M Jr, Mody I, Black DL. 2011. The splicing regulator Rbfox1 (A2BP1) controls neuronal excitation in the mammalian brain. *Nat Genet* **43:** 706–711.

Grabowski PJ. 2005. Splicing-active nuclear extracts from rat brain. *Methods* **37:** 323–330.

Grieco TM, Malhotra JD, Chen C, Isom LL, Raman IM. 2005. Open-channel block by the cytoplasmic tail of sodium channel β4 as a mechanism for resurgent sodium current. *Neuron* **45:** 233–244.

Hammock EA, Levitt P. 2011. Developmental expression mapping of a gene implicated in multiple neurodevelopmental disorders, A2bp1 (Fox1). *Dev Neurosci* **33:** 64–74.

Hausser M, Clark BA. 1997. Tonic synaptic inhibition modulates neuronal output pattern and spatiotemporal synaptic integration. *Neuron* **19:** 665–678.

Huh GS, Hynes RO. 1994. Regulation of alternative pre-mRNA splicing by a novel repeated hexanucleotide element. *Genes Dev* **8:** 1561–1574.

Jensen KB, Dredge BK, Stefani G, Zhong R, Buckanovich RJ, Okano HJ, Yang YY, Darnell RB. 2000. Nova-1 regulates neuron-specific alternative splicing and is essential for neuronal viability. *Neuron* **25:** 359–371.

Jin Y, Suzuki H, Maegawa S, Endo H, Sugano S, Hashimoto K, Yasuda K, Inoue K. 2003. A vertebrate RNA-binding protein Fox-1 regulates tissue-specific splicing via the pentanucleotide GCAUG. *EMBO J* **22:** 905–912.

Kanadia RN, Johnstone KA, Mankodi A, Lungu C, Thornton CA, Esson D, Timmers AM, Hauswirth WW, Swanson MS. 2003. A muscleblind knockout model for myotonic dystrophy. *Science* **302:** 1978–1980.

Kim KK, Adelstein RS, Kawamoto S. 2009. Identification of neuronal nuclei (NeuN) as Fox-3, a new member of the Fox-1 gene family of splicing factors. *J Biol Chem* **284:** 31052–31061.

Kim KK, Kim YC, Adelstein RS, Kawamoto S. 2011. Fox-3 and PSF interact to activate neural cell-specific alternative splicing. *Nucleic Acids Res* **39:** 3064–3078.

Koch S, Strasser V, Hauser C, Fasching D, Brandes C, Bajari TM, Schneider WJ, Nimpf J. 2002. A secreted soluble form of ApoE receptor 2 acts as a dominant-negative receptor and inhibits Reelin signaling. *EMBO J* **21:** 5996–6004.

Kuroyanagi H. 2009. Fox-1 family of RNA-binding proteins. *Cell Mol Life Sci* **66:** 3895–3907.

Larouche M, Beffert U, Herz J, Hawkes R. 2008. The Reelin receptors Apoer2 and Vldlr coordinate the patterning of Purkinje cell topography in the developing mouse cerebellum. *PLoS One* **3:** e1653. doi: 10.1371/journal.pone.0001653.

Lee JA, Tang ZZ, Black DL. 2009. An inducible change in Fox-1/A2BP1 splicing modulates the alternative splicing of downstream neuronal target exons. *Genes Dev* **23:** 2284–2293.

Levin SI, Khaliq ZM, Aman TK, Grieco TM, Kearney JA, Raman IM, Meisler MH. 2006. Impaired motor function in mice with cell-specific knockout of sodium channel Scn8a (NaV1.6) in cerebellar purkinje neurons and granule cells. *J Neurophysiol* **96:** 785–793.

Li Q, Lee JA, Black DL. 2007. Neuronal regulation of alternative pre-mRNA splicing. *Nat Rev Neurosci* **8:** 819–831.

Licatalosi DD, Darnell RB. 2006. Splicing regulation in neurologic disease. *Neuron* **52:** 93–101.

Lim LP, Sharp PA. 1998. Alternative splicing of the fibronectin EIIIB exon depends on specific TGCATG repeats. *Mol Cell Biol* **18:** 3900–3906.

Lim J, Hao T, Shaw C, Patel AJ, Szabo G, Rual JF, Fisk CJ, Li N, Smolyar A, Hill DE, et al. 2006. A protein-protein interaction network for human inherited ataxias and disorders of Purkinje cell degeneration. *Cell* **125:** 801–814.

Lipscombe D. 2005. Neuronal proteins custom designed by alternative splicing. *Curr Opin Neurobiol* **15:** 358–363.

Lukong KE, Richard S. 2008. Motor coordination defects in mice deficient for the Sam68 RNA-binding protein. *Behav Brain Res* **189:** 357–363.

Martin CL, Duvall JA, Ilkin Y, Simon JS, Arreaza MG, Wilkes K, Alvarez-Retuerto A, Whichello A, Powell CM, Rao K, et al. 2007. Cytogenetic and molecular characterization of A2BP1/FOX1 as a candidate gene for autism. *Am J Med Genet B Neuropsychiatr Genet* **144B:** 869–876.

Matlin AJ, Clark F, Smith CW. 2005. Understanding alternative splicing: Towards a cellular code. *Nat Rev Mol Cell Biol* **6:** 386–398.

McGlincy NJ, Tan LY, Paul N, Zavolan M, Lilley KS, Smith CW. 2010. Expression proteomics of UPF1 knockdown in HeLa cells reveals autoregulation of hnRNP A2/B1 mediated by alternative splicing resulting in nonsense-mediated mRNA decay. *BMC Genomics* **11:** 565. doi: 10.1186/1471-2164-11-565.

McKee AE, Minet E, Stern C, Riahi S, Stiles CD, Silver PA. 2005. A genome-wide in situ hybridization map of RNA-binding proteins reveals anatomically restricted expression in the

developing mouse brain. *BMC Dev Biol* **5:** 14. doi: 10.1186/1471-213X-5-14.
Meisler MH, Kearney J, Escayg A, MacDonald BT, Sprunger LK. 2001. Sodium channels and neurological disease: Insights from Scn8a mutations in the mouse. *Neuroscientist* **7:** 136–145.
Miyata T, Nakajima K, Mikoshiba K, Ogawa M. 1997. Regulation of Purkinje cell alignment by reelin as revealed with CR-50 antibody. *J Neurosci* **17:** 3599–3609.
Modafferi EF, Black DL. 1997. A complex intronic splicing enhancer from the c-src pre-mRNA activates inclusion of a heterologous exon. *Mol Cell Biol* **17:** 6537–6545.
Nakahata S, Kawamoto S. 2005. Tissue-dependent isoforms of mammalian Fox-1 homologs are associated with tissue-specific splicing activities. *Nucleic Acids Res* **33:** 2078–2089.
Nilsen TW, Graveley BR. 2010. Expansion of the eukaryotic proteome by alternative splicing. *Nature* **463:** 457–463.
O'Brien JE, Drews VL, Jones JM, Dugas JC, Barres BA, Meisler MH. 2011. Rbfox proteins regulate alternative splicing of neuronal sodium channel SCN8A. *Mol Cell Neurosci* **49:** 120–126.
Plummer NW, McBurney MW, Meisler MH. 1997. Alternative splicing of the sodium channel SCN8A predicts a truncated two-domain protein in fetal brain and non-neuronal cells. *J Biol Chem* **272:** 24008–24015.
Ponthier JL, Schluepen C, Chen W, Lersch RA, Gee SL, Hou VC, Lo AJ, Short SA, Chasis JA, Winkelmann JC, et al. 2006. Fox-2 splicing factor binds to a conserved intron motif to promote inclusion of protein 4.1R alternative exon 16. *J Biol Chem* **281:** 12468–12474.
Raj B, O'Hanlon D, Vessey JP, Pan Q, Ray D, Buckley NJ, Miller FD, Blencowe BJ. 2011. Cross-regulation between an alternative splicing activator and a transcription repressor controls neurogenesis. *Mol Cell* **43:** 843–850.
Raman IM, Bean BP. 1997. Resurgent sodium current and action potential formation in dissociated cerebellar Purkinje neurons. *J Neurosci* **17:** 4517–4526.
Raman IM, Sprunger LK, Meisler MH, Bean BP. 1997. Altered subthreshold sodium currents and disrupted firing patterns in Purkinje neurons of Scn8a mutant mice. *Neuron* **19:** 881–891.
Rice DS, Curran T. 2001. Role of the reelin signaling pathway in central nervous system development. *Annu Rev Neurosci* **24:** 1005–1039.
Robledo RF, Ciciotte SL, Gwynn B, Sahr KE, Gilligan DM, Mohandas N, Peters LL. 2008. Targeted deletion of α-adducin results in absent β- and γ-adducin, compensated hemolytic anemia, and lethal hydrocephalus in mice. *Blood* **112:** 4298–4307.
Ruggiu M, Herbst R, Kim N, Jevsek M, Fak JJ, Mann MA, Fischbach G, Burden SJ, Darnell RB. 2009. Rescuing Z^+ agrin splicing in Nova null mice restores synapse formation and unmasks a physiologic defect in motor neuron firing. *Proc Natl Acad Sci* **106:** 3513–3518.
Sebat J, Lakshmi B, Malhotra D, Troge J, Lese-Martin C, Walsh T, Yamrom B, Yoon S, Krasnitz A, Kendall J, et al. 2007. Strong association of de novo copy number mutations with autism. *Science* **316:** 445–449.
Shibata H, Huynh DP, Pulst SM. 2000. A novel protein with RNA-binding motifs interacts with ataxin-2. *Hum Mol Genet* **9:** 1303–1313.
Smith SL, Otis TS. 2005. Pattern-dependent, simultaneous plasticity differentially transforms the input-output relationship of a feedforward circuit. *Proc Natl Acad Sci* **102:** 14901–14906.
Sugnet CW, Srinivasan K, Clark TA, O'Brien G, Cline MS, Wang H, Williams A, Kulp D, Blume JE, Haussler D, et al. 2006. Unusual intron conservation near tissue-regulated exons found by splicing microarrays. *PLoS Comput Biol* **2:** e4. doi: 10.1371/journal.pcbi.0020004.
Sun S, Zhang Z, Sinha R, Karni R, Krainer AR. 2010. SF2/ASF autoregulation involves multiple layers of post-transcriptional and translational control. *Nat Struct Mol Biol* **17:** 306–312.
Tang ZZ, Zheng S, Nikolic J, Black DL. 2009. Developmental control of CaV1.2 L-type calcium channel splicing by Fox proteins. *Mol Cell Biol* **29:** 4757–4765.
Thompson PM, Gotoh T, Kok M, White PS, Brodeur GM. 2003. CHD5, a new member of the chromodomain gene family, is preferentially expressed in the nervous system. *Oncogene* **22:** 1002–1011.
Tronche F, Kellendonk C, Kretz O, Gass P, Anlag K, Orban PC, Bock R, Klein R, Schutz G. 1999. Disruption of the glucocorticoid receptor gene in the nervous system results in reduced anxiety. *Nat Genet* **23:** 99–103.
Ule J, Ule A, Spencer J, Williams A, Hu JS, Cline M, Wang H, Clark T, Fraser C, Ruggiu M, et al. 2005. Nova regulates brain-specific splicing to shape the synapse. *Nat Genet* **37:** 844–852.
Underwood JG, Boutz PL, Dougherty JD, Stoilov P, Black DL. 2005. Homologues of the *Caenorhabditis elegans* Fox-1 protein are neuronal splicing regulators in mammals. *Mol Cell Biol* **25:** 10005–10016.
Voineagu I, Wang X, Johnston P, Lowe JK, Tian Y, Horvath S, Mill J, Cantor RM, Blencowe BJ, Geschwind DH. 2011. Transcriptomic analysis of autistic brain reveals convergent molecular pathology. *Nature* **474:** 380–384.
Wang VY, Zoghbi HY. 2001. Genetic regulation of cerebellar development. *Nat Rev Neurosci* **2:** 484–491.
Wang HY, Xu X, Ding JH, Bermingham JR Jr, Fu XD. 2001. SC35 plays a role in T cell development and alternative splicing of CD45. *Mol Cell* **7:** 331–342.
Wolf HK, Buslei R, Schmidt-Kastner R, Schmidt-Kastner PK, Pietsch T, Wiestler OD, Blumcke I. 1996. NeuN: A useful neuronal marker for diagnostic histopathology. *J Histochem Cytochem* **44:** 1167–1171.
Xu X, Yang D, Ding JH, Wang W, Chu PH, Dalton ND, Wang HY, Bermingham JR Jr, Ye Z, Liu F, et al. 2005. ASF/SF2-regulated CaMKIIδ alternative splicing temporally reprograms excitation-contraction coupling in cardiac muscle. *Cell* **120:** 59–72.
Yang G, Huang SC, Wu JY, Benz EJ Jr. 2008. Regulated Fox-2 isoform expression mediates protein 4.1R splicing during erythroid differentiation. *Blood* **111:** 392–401.
Yano M, Hayakawa-Yano Y, Mele A, Darnell RB. 2010. Nova2 regulates neuronal migration through an RNA switch in disabled-1 signaling. *Neuron* **66:** 848–858.
Yeo GW, Xu X, Liang TY, Muotri AR, Carson CT, Coufal NG, Gage FH. 2007. Alternative splicing events identified in human embryonic stem cells and neural progenitors. *PLoS Comput Biol* **3:** 1951–1967.
Yeo GW, Coufal NG, Liang TY, Peng GE, Fu XD, Gage FH. 2009. An RNA code for the FOX2 splicing regulator revealed by mapping RNA-protein interactions in stem cells. *Nat Struct Mol Biol* **16:** 130–137.
Zhang C, Zhang Z, Castle J, Sun S, Johnson J, Krainer AR, Zhang MQ. 2008. Defining the regulatory network of the tissue-specific splicing factors Fox-1 and Fox-2. *Genes Dev* **22:** 2550–2563.
Zheng S, Gray EE, Chawla G, Porse BT, O'Dell TJ, Black DL. 2012. PSD-95 is post-transcriptionally repressed during early neural development by PTBP1 and PTBP2. *Nat Neurosci* doi: 10.1038/nn.3026.